Grounding line movement and ice shelf buttressing in marine ice sheets

Grounding line movement and ice shelf buttressing in marine ice sheets

D. Goldberg,[1] D. M. Holland,[1] and C. Schoof[2]

Received 16 December 2008; revised 29 April 2009; accepted 24 July 2009; published 23 December 2009.

[1] Understanding the dynamics of marine ice sheets is integral to studying the evolution of the Antarctic ice sheet in both the short and long terms. An important component of the dynamics, grounding line migration, has proved difficult to represent in numerical models, and most successful attempts have made use of techniques that are only readily applicable to flow line models. However, to capture the stress transmission involved in another important component, the buttressing of a marine ice sheet by its ice shelf, the transverse direction must also be resolved. We introduce a model that solves the time-dependent shelfy stream equations and makes use of mesh adaption techniques to overcome the difficulties typically associated with the numerics of grounding line migration. We compare the model output with a recent benchmark for flow line models and show that our model yields an accurate solution while using far less resources than would be required without mesh adaption. We also show that the mesh adapting techniques extend to two horizontal dimensions. Experiments are carried out to determine how both ice shelf buttressing and ice rises affect the marine instability predicted for an ice sheet on a foredeepened bed. We find that buttressing is not always sufficient to stabilize such a sheet but collapse of the grounded portion is still greatly delayed. We also find that the effect of an ice rise is similar to that of narrowing the ice shelf.

Citation: Goldberg, D., D. M. Holland, and C. Schoof (2009), Grounding line movement and ice shelf buttressing in marine ice sheets, *J. Geophys. Res.*, *114*, F04026, doi:10.1029/2008JF001227.

1. Introduction

[2] The past decade has seen huge advances in our ability to observe global and regional mass budgets of the Earth's cryosphere, and some concerning trends have arisen from the data. The West Antarctic Ice Sheet (WAIS), an ice mass large enough to raise ocean levels by more than 5 m were it to collapse [*Mercer*, 1978], lost between 47 and 59 Gt of ice per year during the 1990s [*Shepherd and Wingham*, 2007]. A large portion of grounded ice loss was from the Amundsen Sea sector of the WAIS, notably Pine Island (PIG) and Thwaites (TG) glaciers. While glacial mass budget is subject to variability in both accumulation/ablation and ice discharge, *Shepherd et al.* [2002] found that climatic variability was too small to explain the mass loss, and it was ice dynamic effects that were responsible. *Shepherd et al.* [2004] found that during the same time period, the floating ice shelves fed by the Amundsen Sector glaciers suffered enormous mass loss, some shelves losing up to 7% of their thickness over a 9-year period. It is now thought that there may be a connection between the ice shelf mass loss and the loss of inland ice. The connection between the thinning of an ice shelf or ice tongue and speedup of grounded ice has also been supported by recent observations in Greenland [*Krabill et al.*, 2000; *Joughin et al.*, 2004; *Holland et al.*, 2008].

[3] Such a large mass imbalance in West Antarctica is of societal significance because it contributes to sea level rise (SLR). Since ice shelves are almost perfectly buoyed by the ocean according to Archimedes' Principle [*Van der Veen*, 1999], the WAIS contribution to sea level rise is almost entirely due to changes in the mass of grounded ice [*Jenkins and Holland*, 2007]. These changes can result from thickness evolution and from changes in grounded extent associated with movement of the grounding line (the boundary between floating and grounded ice). Both thinning and grounding line retreat have been observed in West Antarctica in recent years [*Rignot et al.*, 2002].

[4] Inland retreat of the grounding line may be an indicator of accelerating mass loss in the future. Much of the West Antarctic ice mass is a marine ice sheet, meaning its base is below sea level [*Mercer*, 1978], and more significantly still, the WAIS rests on an upsloping (or foredeepened) bed that is deeper below sea level in the center of the ice sheet than at the grounding line. For several decades, concerns have been raised over the stability of such ice sheets: based on a simplified model, *Weertman* [1974] predicted that a two-dimensional marine ice sheet resting on a bed can only be in a stable, steady state if the bed is downsloping and does not exceed a critical depth. A similar model was used by *Thomas* [1977] to argue that a

[1]Courant Institute of Mathematical Sciences, New York University, New York, New York, USA.
[2]Department of Earth and Ocean Sciences, University of British Columbia, Vancouver, British Columbia, Canada.

0148-0227/09/2008JF001227

grounding line resting in steady state on an foredeepened bed will retreat unstably if perturbed, and by *Thomas and Bentley* [1978] to argue that the WAIS is therefore unstable.

[5] Since then, the dynamics of grounding lines in sheet/stream shelf systems have been closely examined in a variety of models that differ in their model geometries, model resolution, numerical discretization and so forth, with differing views on how to best represent the physics, and often yielding mutually inconsistent results. Some of the inconsistencies between models can be traced to the mechanical coupling between ice sheets and ice shelves. Ice shelves are dominated by longitudinal deviatoric stresses (i.e., by deviatoric normal stresses), while vertical shear and basal friction generally dominate force balance in grounded ice sheets. A crucial issue facing marine ice sheet models is how to couple these mechanically distinct flows at the grounding line: what continuity conditions should be applied at the grounding line?

[6] The early calculations of *Weertman* [1974], *Thomas* [1977], and *Thomas and Bentley* [1978] applied a "zero-order" approach in which longitudinal stresses do not play a role in the force balance of the grounded sheet, and the ice shelf is coupled to the ice sheet by imposing continuity in the longitudinal derivative of vertically averaged velocity as a proxy for the continuity of longitudinal stress. A more refined approach adopted by the models of *Chugunov and Wilchinsky* [1996], *Wilchinsky and Chugunov* [2000], and *Schoof* [2007a] and supported on observational grounds by *Mayer and Huybrechts* [1999] is that a transition zone exists near the grounding line where all stress terms dominant in either the sheet or the shelf are important. Depending on various factors, this zone can have a length scale ranging from one to many ice thicknesses [*Chugunov and Wilchinsky*, 1996; *Pattyn et al.*, 2006; *Schoof*, 2007a; *Nowicki and Wingham*, 2007] and its importance to the large-scale system dynamics of marine ice sheets has been debated. Early work by *Thomas* [1985] and *Van der Veen* [1985] included parameterizations of the transition zone of differing levels of sophistication, with both supporting Weertman's original marine ice sheet instability mechanism. *Hindmarsh* [1996], on the other hand, argued that the narrow transition zone between grounded sheet and floating shelf should effectively decouple the two, and that stresses in the ice shelf should have no effect on the flow of the grounded sheet or the migration of the grounding line. Based on this, he promoted the concept of "neutral stability" for a marine ice sheet, implying that possible steady state grounding line positions were essentially unconstrained, and a perturbation in grounding line position would not lead to unstable retreat or advance for a foredeepened bed, nor to a return to the original grounding line position for a downsloping bed. *Pattyn et al.* [2006], using a higher-order model in which the scale of the transition zone was imposed through a strong increase in basal friction away from the grounding line, reproduced Hindmarsh's neutrally stable behavior in the special case of a vanishing transition zone, but found discrete, stable steady states on downsloping beds as the transition zone widened, and no stable steady states for an upward-sloping bed.

[7] The discrepancies between these models can partly be attributed to their different representations of ice flow mechanics near the grounding line. A second issue that can obscure the effect of different model physics is the robustness of numerical models to changes in discretization schemes, resolution and so on. This was studied in depth by *Vieli and Payne* [2005]. They found that both steady states calculated for a given climate and responses to climatic perturbations depended heavily on the type of model physics used, and on numerical details of the model such as discretization schemes and grid size.

[8] The recent work of *Schoof* [2007a, 2007b] has tried to address both the role of the sheet-shelf transition zone in overall marine ice sheet dynamics and numerical artifacts associated with grid resolution. Using the technique of matched asymptotic expansions, Schoof argues that the transition zone does control grounding line movement, even if its horizontal extent is very limited and longitudinal stresses play an insignificant role in most of the ice sheet. His results provide a subgrid parameterization of ice flow in the transition zone that confirms Weertman's argument that mass flux through the grounding line is an increasing function of ice thickness at the grounding line, from which the instability hypothesis for marine ice sheets follows. Schoof's results also provide a scaling estimate for the transition zone length in terms of model parameters, and show that the subgrid parameterization of transition zone ice flow is in good agreement with an ultra high-resolution numerical model that resolves the transition zone. As a possible explanation for the inconsistent numerical results obtained by *Vieli and Payne* [2005], *Schoof* [2007b] suggests insufficient resolution of the grounding line transition zone, which may also affect some of the calculations by *Pattyn et al.* [2006].

[9] The models reviewed so far are either 1-D or 2-D planar models: the horizontal direction perpendicular to the flow direction (the transverse direction) plays no role in the dynamics of the ice sheet. (For ease of discussion, the reader is referred to Table 1, which gives the naming convention used in this text for the physical and mathematical dimensionality of ice models, with examples. Note this list is not intended to be exhaustive.) Real ice sheets, of course, have two horizontal directions, and this adds a further set of complications. Not only do the questions raised above (how the sheet-shelf transition zone affects the flow, and how to resolve its effect accurately in numerical models) remain, but the effect of stresses associated with shearing in the direction transverse to the main flow (so-called lateral shear stresses) must also be accounted for.

[10] Weertman's instability hypothesis is based on the notion that ice flux through the grounding line increases with ice thickness there. More subtly, ice flux at the grounding line in his model is actually an increasing function of both, ice thickness and longitudinal stress [see also *Schoof*, 2007b, section 4.2]. However, for a 1-D ice shelf (with no lateral shear) it can be shown that longitudinal stress itself is an increasing function of ice thickness in the shelf and in particular at the grounding line [e.g., *MacAyeal and Barcilon*, 1988]. Consequently, Weertman's result of flux as a function of ice thickness does hold, and the actual shape of the ice shelf (its extent and its profile) does not affect the dynamics of the grounded sheet.

[11] The same is not true for a three-dimensional marine ice sheet. Here, longitudinal stress at the grounding line will generally not be a function of ice thickness, but will be

Table 1. Naming Convention for Ice Sheet Models, With Respect to Dimensionality, Both in Physical Representation and Resolution of Velocities[a]

Type	Physical Dimension	Flow Regime	Along-Flow Direction	Transverse Direction	Vertical Direction	Example
1D	2-D	plug or shear	resolved	ignored	parameterized	*Vieli and Payne* [2005]
Quasi 2-D	3-D	plug	resolved	parameterized	parameterized	*Dupont* [2004]
2-D planar	2-D	N/A	resolved	ignored	resolved	*Pattyn et al.* [2006]
Quasi 3-D	3-D	N/A	resolved	parameterized	resolved	*Pattyn* [2002]
2-D	3-D	plug	resolved	resolved	parameterized	*MacAyeal* [1989]
3-D	3-D	N/A	resolved	resolved	resolved	*Blatter* [1995]

[a]Plug flow means the velocity field does not depend on depth in the flow; shear means only vertical shear stress is modeled; and N/A means all are considered. The models considered in this study are 1-D (plug) and 2-D.

reduced by the action of lateral shear stresses that now account for some of the driving stress acting on the sheet. *Dupont and Alley* [2005] used a quasi 2-D stream shelf model in which transverse effects were parameterized to demonstrate this so-called buttressing effect of a confined ice shelf, and went on to suggest that stable steady states on foredeepened beds are possible if lateral shearing in the ice shelf is sufficiently strong.

[12] *Shepherd et al.* [2004] suggest loss of buttressing as a mechanism for how erosion of the Amundsen Sea ice shelves by ocean circulation could cause the heightened mass discharge observed in the Amundsen Sector of the WAIS. This mechanism's viability has been demonstrated through numerical experiments for Pine Island Glacier (PIG). *Schmeltz et al.* [2002], using a 2-D model based on *MacAyeal* [1989] with ice geometry and model parameters appropriate to the PIG, showed that a loss of ice shelf area results in a sizable increase in ice velocity at the grounding line, although responses farther inland are smaller. However, this study only evaluated instantaneous velocity response of the ice stream to the removal of the ice sheet, and did not study the subsequent evolution of the ice stream. Using a time-dependent 2-D model (forced with parameters that were inverse modeled using a static 3-D model), *Payne et al.* [2004] showed inland transient response to perturbations at or near the grounding line can explain the observed variability in thickness evolution. However, their study did not include dynamic grounding line movement, and was therefore not able to predict whether the unstable feedback that underlies Weertman's instability would occur at PIG, whose bed is significantly foredeepened.

[13] In this paper we aim to address the three issues identified above for a three-dimensional ice sheet: the effect of the transition from sheet to shelf flow, the need for a numerically robust model that resolves this transition zone, and the effect of lateral shearing (or buttressing) in a three-dimensional ice sheet. To this end, we introduce a dynamical model of a three-dimensional marine ice sheet with a migrating grounding line. The model is based on the depth-integrated model of *MacAyeal* [1989] and therefore falls in the "2-D flow regime" category of Table 1. Our numerical approach is novel in that it uses higher resolution in locations where it is needed (such as the transition zone near the grounding line), and that it dynamically adapts the computational mesh as these locations change in order to limit computational expense. The model has two different modes of mesh adaption, which we term moving mesh and adaptive refinement. It is shown that, in the special case of a 1-D system, our model overcomes the difficulties discussed by *Vieli and Payne* [2005], and that it agrees well with the quasi-analytic results of *Schoof* [2007a]. It is further shown that no numerical difficulties, such as strong dependence on grid size or initial conditions, present themselves in a 2-D simulation, even though our computational requirements remain modest. We then apply our model to a marine ice sheet shelf system on a foredeepened bed with rigid sidewalls and investigate the conditions under which the buttressing provided by sidewalls is sufficient to prevent Weertman's unstable collapse. The ability of each mode of mesh adaption to provide a reliable solution under a variety of conditions is also evaluated.

2. Shelfy Stream Model

2.1. Model Equations

[14] We consider a marine ice sheet that consists of a grounded portion sliding over its bed, and an attached ice shelf. Based on the assumption that slip at the base of the ice is fast compared with shearing across the ice thickness, *MacAyeal* [1989] derived the following model for the horizontal components u and v of ice velocity:

$$\partial_x\left(4h\nu u_x + 2h\nu v_y\right) + \partial_y\left(h\nu\left(u_y + v_x\right)\right) - \tau_b^x = \rho g h s_x, \qquad (1)$$

$$\partial_y\left(4h\nu v_y + 2h\nu u_x\right) + \partial_x\left(h\nu\left(u_y + v_x\right)\right) - \tau_b^y = \rho g h s_y, \qquad (2)$$

$$\nu = A^{-1/n}\left|u_x^2 + v_y^2 + u_x v_y + \frac{1}{4}\left(u_y + v_x\right)^2\right|^{\frac{1-n}{2n}}. \qquad (3)$$

Here, h is vertical thickness, s is its surface elevation, ρ is density, u and v are x and y velocities, $\vec{\tau}_b$ is basal stress, and A and n are the usual coefficients in Glen's law [*Paterson*, 2001, chapter 5], where we use $n = 3$ in all our numerical computations. The right hand sides of (1) and (2) are subsequently referred to as the driving stress terms. Noting that (1) and (2) are invariant under rotations in the (x, y) plane, the model can be written more compactly as [*Schoof*, 2006]

$$\nabla \cdot \sigma - \vec{\tau}_b = \rho g h \nabla s, \qquad (4)$$

where the tensor σ is defined by

$$\sigma_{ij} = \nu h\left(\frac{\partial u_i}{\partial x_j} + \frac{\partial u_j}{\partial x_i} + 2\delta_{ij}\frac{\partial u_k}{\partial x_k}\right), \qquad (5)$$

where i, j, and k vary over x and y and the summation convention is applied. In this study, temperature and fabric effects are not considered, and A remains constant.

[15] At the lateral domain boundaries, the boundary conditions on the diagnostic equations (1, 2) can either be on velocity or on stress. The former is the case if, for instance, that part of the boundary represents a slow-moving ice ridge or a symmetrical ice divide. If the boundary is an ice shelf front then the balance between internal stresses and hydrostatic stresses within the ice and the ocean gives rise to the following:

$$\sigma_{ij} n_j = \frac{1}{2}\left(1 - \frac{\rho}{\rho_w}\right)\rho g h_f^2 n_i, \tag{6}$$

where h_f is thickness at the front, ρ_w is ocean density, $\vec{n}$ is the outward normal vector (in the x,y plane) at the front, σ is as above, and i, j again vary over x, y [*Huybrechts*, 1990]. (We are ignoring the case where the entire domain is floating and every lateral boundary is an ice/ocean interface. In this case the velocity is only determined up to a uniform translation plus a solid body rotation, and the ice shelf is essentially a large iceberg.)

[16] In the event that part of the shelf front is grounded (on an ice rise, say) then (6) is generalized by replacing $\frac{1}{2}(1 - \frac{\rho}{\rho_w})\rho g h_f^2$ by

$$\frac{1}{2}\rho g\left(h_f^2 - \frac{\rho_w}{\rho} R_f^2\right), \tag{7}$$

where R_f and h_f are the depth of the base and the total thickness at the front, respectively [*Schoof*, 2007b, Appendix B]. Note that in this study we consider only a stationary ice shelf front; that is, we assume that all ice mass that moves across the front is instantly calved and therefore no longer plays a role in the dynamics.

[17] The conditions under which MacAyeal's model is valid also ensure that normal stress at the base of the ice is cryostatic, i.e., that the normal stress at the base is equal to the weight of the ice column above it [*MacAyeal*, 1989, Appendix A]. This means that a simple criterion determines whether ice is floating or grounded:

$$\rho h + \rho_w R(x,y) \begin{cases} \le 0 & \text{for floating ice,} \\ > 0 & \text{for grounded ice,} \end{cases} \tag{8}$$

where R is bedrock elevation, defined to be negative if below sea level. This flotation condition simply states that the ice will float when ocean pressure at the base can support the weight of the overlying ice column, and that it is in contact with the bed otherwise. The assumption is made here that ocean water at hydrostatic pressure is always available to support a column's weight when it can do so. Ice surface elevation is then related to ice thickness through

$$s = \begin{cases} \left(1 - \dfrac{\rho}{\rho_w}\right) h & \text{where } \rho h + \rho_w R \le 0 \\ R + h & \text{where } \rho h + \rho_w R > 0. \end{cases} \tag{9}$$

Furthermore, there is no basal stress where ice is floating. In areas where ice is grounded, the form of $\vec{\tau}_b$ depends on conditions at the base of the ice stream, which are a subject of debate for many West Antarctic ice streams. Here we choose a parameterization corresponding to ice sliding over rigid bedrock [*Fowler*, 1981], which yields

$$\vec{\tau}_b = \begin{cases} 0 & \text{where } \rho h + \rho_w R \le 0 \\ C|\vec{u}|^{m-1}\vec{u} & \text{where } \rho h + \rho_w R > 0, \end{cases} \tag{10}$$

where m is a positive constant and C is a parameter. In general C is spatially nonuniform and is dependent upon factors such as bed roughness and effective pressure [*Paterson*, 2001, chapter 7]. To simplify matters, we make C spatially uniform in our study, but allowing for spatially and temporally varying C is an avenue of further research.

[18] The thickness field evolves in time according to the vertically integrated incompressibility condition, taking into account mass balance terms at the upper and lower surfaces (e.g., snow accumulation, melting, and accretion), represented by a:

$$h_t + \nabla \cdot (\vec{u}h) = a. \tag{11}$$

Since temperature and other material properties are not modeled, h is the only prognostic variable in the system.

[19] When applied to grounded ice, the model above is often called the shelfy stream model, and the "shallow shelf" model for floating ice. It has been widely used, at varying levels of complexity, to model portions of West Antarctica [e.g., *MacAyeal*, 1989; *Hulbe*, 1998; *Schmeltz et al.*, 2002; *Payne et al.*, 2004].

2.2. Nondimensionalization and Buttressing

[20] For the remainder of the paper we give dimensional results, but it is instructive to briefly consider the nondimensionalized system of equations. Details are found in the work of *Schoof* [2007a], but briefly, if variables are scaled with the assumption that, over most of the grounded domain, the dominant balance is between driving force and basal friction, the nondimensionalized equations are

$$\begin{gathered} \varepsilon\hat{\nabla}\cdot\hat{\sigma} - \chi_g|\hat{\mathrm{u}}|^{m-1}\hat{\vec{u}} = \hat{h}\hat{\nabla}\Big(\chi_g(1-r)\hat{h} + \big(1-\chi_g\big)(\hat{R}+\hat{h})\Big), \\ \hat{\sigma}_{ij} = \hat{\nu}\left(\frac{\partial\hat{u}_i}{\partial\hat{x}_j} + \frac{\partial\hat{u}_j}{\partial\hat{x}_i} + 2\delta_{ij}\big(\hat{u}_{\hat{x}} + \hat{v}_{\hat{y}}\big)\right), \end{gathered} \tag{12}$$

$$\begin{gathered} \hat{\nu} = \left|\hat{u}_{\hat{x}}^2 + \hat{v}_{\hat{y}}^2 + \hat{u}_{\hat{x}}\hat{v}_{\hat{y}} + \frac{1}{4}\big(\hat{u}_{\hat{y}} + \hat{v}_{\hat{x}}\big)^2\right|^{\frac{1-n}{2n}}, \\ \hat{h}_{\hat{t}} + \hat{\nabla}\Big(\hat{u}\hat{h}\Big) = \hat{a}. \end{gathered} \tag{13}$$

Here χ_g is equal to 1 where $r\hat{h} + \hat{R} > 0$ (i.e., where the floatation condition is not satisfied), and 0 otherwise. Hats appear over nondimensionalized variables, which are of order unity, and $r = \rho_i/\rho_w$. The dimensionless number ε has the form

$$\varepsilon = \frac{A^{-\frac{1}{n}}([u]/[x])^{\frac{1}{n}}}{2\rho g[h]}, \tag{14}$$

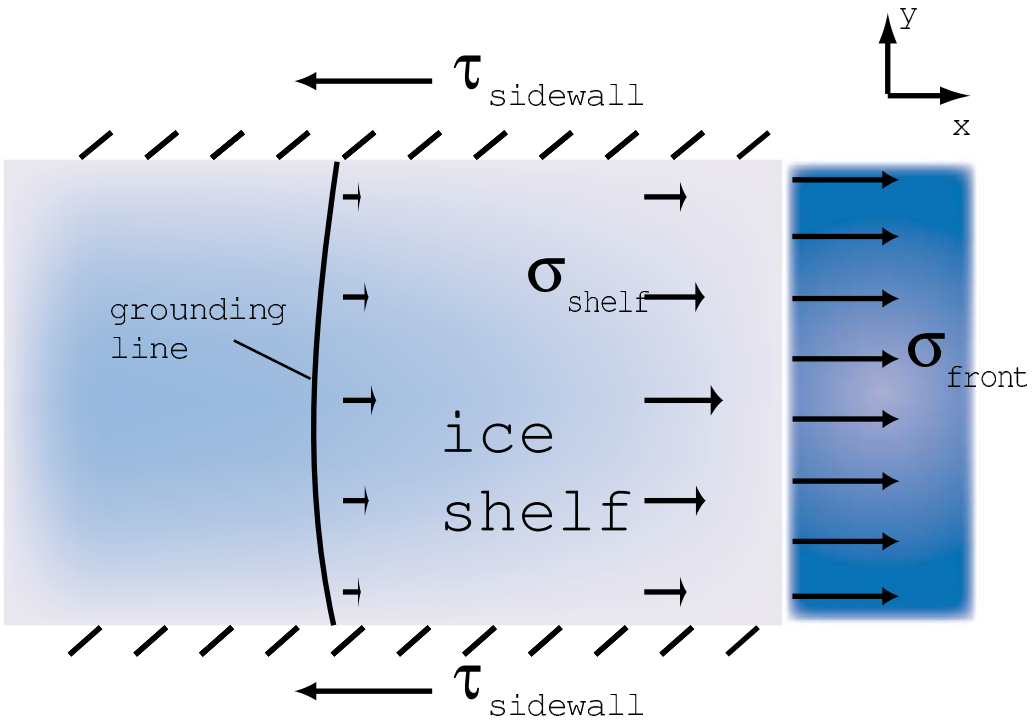

Figure 1. Schematic illustration of buttressing. Part of the stress applied by the ocean at the shelf front (σ_{front}) is taken up by sidewall stress (τ_{sidewall}), and so longitudinal stresses within the shelf (σ_{shelf}) are small at the grounding line.

where $[x]$, $[h]$, and $[u]$ are characteristic scales of length, thickness, and velocity, respectively. ε can be thought of as the ratio of the scale of the axial deviatoric stress in the grounded domain to the overburden pressure.

[21] The parameter ε is quite small for typical ice stream conditions in Antarctica, as is shown by considering studies of two representative West Antarctica ice streams. An observational study of Rutford Ice Stream by *Frolich et al.* [1987] gives representative scales of $[u] = 300$ ma^{-1}, $[h] = 2 \times 10^3$ m, $[x] = 2 \times 10^4$ m (in the transverse direction), and the Glen's law constant A used was equal to 1.6×10^{-17} Pa^{-3} a^{-1}. This gives $\varepsilon \approx 0.0024$. In a modeling study of Pine Island Glacier [*Payne et al.*, 2004], the representative scales were $[u] = 2 \times 10^3$ ma^{-1}, $[h] = 1.5 \times 10^3$ m, $[x] = 2 \times 10^5$ m (in the along-flow direction), and, using a representative Glen's law constant of 4×10^{-18} Pa^{-3} a^{-1} [*Dupont and Alley*, 2005], this gives $\varepsilon \approx 0.0045$.

[22] At the grounding line, ice velocity $\hat{u}_i$, ice thickness $\hat{h}$ and viscous stresses ($\varepsilon\hat{\sigma}_{ij}n_j$) are continuous, where n_j is normal to the grounding line; that is, these stresses must ensure force balance in the shelf. In a completely unbuttressed shelf, the integrated effect of gravity on the shelf is felt in full at the grounding line, and the average value of the longitudinal stress normal to the grounding line is $\frac{1}{2}(1 - \frac{\rho}{\rho_w})\hat{h}^2$. This is independent of ε, yet when $\varepsilon \ll 1$ lateral viscous stresses are negligible in the interior of the grounded sheet, and so there is a stress boundary layer near the grounding line (often called the sheet-shelf transition zone). Buttressing occurs when stresses at the lateral shelf boundaries reduce the longitudinal stress required at the grounding line in closing the ice shelf force balance as illustrated in Figure 1.

[23] It is also instructive to see the dependence of ε in terms of domain and system parameters. With $n = 3$, $m = 1/3$, it can be shown [*Schoof*, 2007a]

$$\varepsilon \propto A^{-.33} C^{-.57} [x]^{-.76} [a]^{.14}, \tag{15}$$

where $[a]$ is the scale of the accumulation rate. From (15) it can be seen that weaker ice (larger A) and a stronger base (larger C) decrease ε.

3. Numerics

3.1. Momentum Balance

[24] In the model, the diagnostic equations for velocity ((1) and (2)) are solved using finite elements. The mesh is composed of quadrilateral cells, and cell-wise bilinear nodal basis functions are used, which are of sufficient polynomial order for this problem [*Schoof*, 2006]. Integration of nonlinear terms such as viscosity and basal traction is done using Gaussian quadrature.

[25] The nonlinear, elliptic system ((1) and (2)) is solved iteratively for velocities using Picard-type fixed point iteration, or "iteration on viscosity" [e.g., *MacAyeal and Thomas*, 1986; *Reist*, 2005]:

$$\partial_x\left(4h\nu^{i-1}u_x^i + 2h\nu^{i-1}v_y^i\right) + \partial_y\left(h\nu^{i-1}\left(u_y^i + v_x^i\right)\right) - \chi_g C|\vec{u}^{i-1}|^{m-1}u^i = \rho g h s_x \tag{16}$$

and a similar equation corresponding to (2). Here the updated velocity iterates u^i, v^i are the only unknowns, and $\chi_g = 1$ where ice is grounded, and 0 otherwise as before.

The stopping condition for this iteration is that the nonlinear residual is sufficiently small relative to its initial value:

$$|M_\nu(\vec{U}^i)\vec{U}^i - \vec{b}| < tol \times |M_\nu(\vec{U}^0)\vec{U}^0 - \vec{b}|. \quad (17)$$

Here M_ν is the stiffness matrix resulting from discretization, b is the discretized driving stress, $\vec{U}$ is the vector of nodal values of velocity, and *tol* is a small number, e.g., 10^{-6} or 10^{-7}. The dependence of M_ν on $\vec{U}$ reflects the dependence of viscosity and nonlinear basal stress on the solution. The linear system at each iteration is solved by conjugate gradients with either a Jacobi or block Jacobi preconditioner.

[26] The only additional complications in solving (1, 2) arise from the difference between the grounded and floating parts of the domain, which is apparent from the discontinuous nature of shear stress gradients in (16) signified by the factor χ_g. Our discretization of (16) is, however, based on the weak form [*Evans*, 1991] of this equation [*Schoof*, 2006], which can easily handle such discontinuities. The weak form of our shelfy stream system of equations in general can be shown to correspond to the minimization of a functional of the form [see *Schoof*, 2006, equation (3.13); *Schoof*, 2009, equations (3.10a and 3.10d)]

$$\begin{aligned} J(u,v) = &\int_\Omega \frac{4nA^{-1/n}}{n+1} h \left| u_x^2 + v_y^2 + u_x v_y + \frac{1}{4}(u_y + v_x)^2 \right|^{\frac{n+1}{n}} \\ &+ \frac{\chi_g C}{m+1} |\vec{u}|^{m+1} + \rho g h \nabla s \cdot \vec{u}\, d\Omega \\ &- \int_{\text{calving front}} \frac{1}{2}\left(1 - \frac{\rho}{\rho_w}\right) g h^2 \vec{n} \cdot \vec{u}\, d\Gamma, \end{aligned} \quad (18)$$

where Ω is the domain. $J(u, v)$ is clearly well defined even with the discontinuities in χ_g and ∇s. Similarly, the weak form of (16) corresponds to the minimization of

$$\begin{aligned} J_P(u^i, v^i) = &\int_\Omega 2\nu^{i-1} h \left[u_x^2 + v_y^2 + u_x v_y + \frac{1}{4}(u_y + v_x)^2 \right] \\ &+ \frac{1}{2}\chi_g C |\vec{u}^{i-1}|^{m-1} |\vec{u}|^2 + \rho g h \nabla s \cdot \vec{u}\, d\Omega \\ &- \int_{\text{calving front}} \frac{1}{2}\left(1 - \frac{\rho}{\rho_w}\right) g h^2 \vec{n} \cdot \vec{u}\, d\Gamma, \end{aligned} \quad (19)$$

which is again well defined even with these discontinuities.

3.2. Mass Balance

[27] The prognostic equation for thickness (11) is solved by a mass-conserving, finite volume method. For the prognostic solution the thickness h is represented as piecewise constant on each cell, rather than continuous piecewise bilinear. This inconsistency is resolved before each new diagnostic solution by interpolation of the piecewise constant solution on to the bilinear finite element space. To advance a time step, mass fluxes at cell boundaries are found using velocities corresponding to the old time step. In some instances, to allow for larger time steps, the scheme is made semiimplicit: thickness values from the new time step are used, but the velocities are still from the old time step.

3.3. Mesh Refinement

[28] We have implemented two different methods of mesh adaption in order to provide higher resolution where it is needed. (In any given model run, only one of the methods is used.) The first is a moving mesh, where the grid points are moved such that they cluster in regions where high resolution is required, while the number and connectivity of grid points is constant (it is sometimes called r refinement). The second is adaptive refinement (so-called h refinement), where cells are divided into smaller cells where extra resolution is required and groups of cells are coarsened into larger cells in regions where lower resolution suffices.

3.3.1. Moving Mesh

[29] In the moving mesh method, the physical domain, with coordinates x and y, is treated as the mapping of a computational domain, with coordinates ξ and η. The grid points of the mesh, defined in (x, y) space, are the mappings of regularly spaced points in (ξ, η) space. The idea is to define a mapping at each time step that provides a mesh in (x, y) space that has closely spaced grid lines where high resolution is required, and smoothly varying cell size. This is accomplished by ensuring that the function $\vec{x}(\xi, \eta)$ satisfies the equation

$$\nabla_{[\xi,\eta]} \cdot \left(\omega \nabla_{[\xi,\eta]} \vec{x}\right) = 0, \quad (20)$$

where $\omega(h(\vec{x}), \vec{x})$ is known as the monitor function, and its functional form has to be chosen such that the mesh has the properties mentioned above. (20) is not solved to a high degree of accuracy at each time step, but rather a few iterations are made using a simple relaxation scheme. Boundary grid points are moved as follows: a point on a y boundary remains on that y boundary, and similarly for x boundaries, and the points are moved along the boundaries through a one-dimensional version of (20). Care needs to be taken that the mesh does not become too distorted, i.e., that $x(\xi, \eta)$ is monotone in ξ for every η and $y(\xi, \eta)$ is monotone in η for every ξ. A candidate for a monitor function is a function of nearest distance to the grounding line:

$$\omega(\vec{x}) = 1 + \frac{\mu_1}{1 + \mu_2^2 \left(dist(\vec{x}, \Gamma_g)\right)^2}, \quad (21)$$

where Γ_g is the grounding line [*Beckett et al.*, 2001]. μ_1 and μ_2 must be chosen appropriately (see 4.1). While this works well for 1-D simulations, finding the distance of all 2-D mesh points to a given contour is again expensive, and the fact that the grounding line must be defined discretely leads to significant distortion in the mesh near the grounding line. A compromise is to use height above floatation as a proxy for distance from the grounding line:

$$\omega(\vec{x}, h) = 1 + \frac{\mu_1}{1 + \mu_2^2 \left(h^*\right)^2}, \quad (22)$$

where $h^* \equiv \frac{\rho}{\rho_w} h + R(\vec{x})$. Note that even with identical values of μ_1, μ_2, (22) will give higher-resolution concentration at the grounding line when h is steeper there.

[30] With each iteration of the relaxation scheme for (20), the physical grid points in (x, y) space shift, and hence thickness h needs to be interpolated from the old mesh to

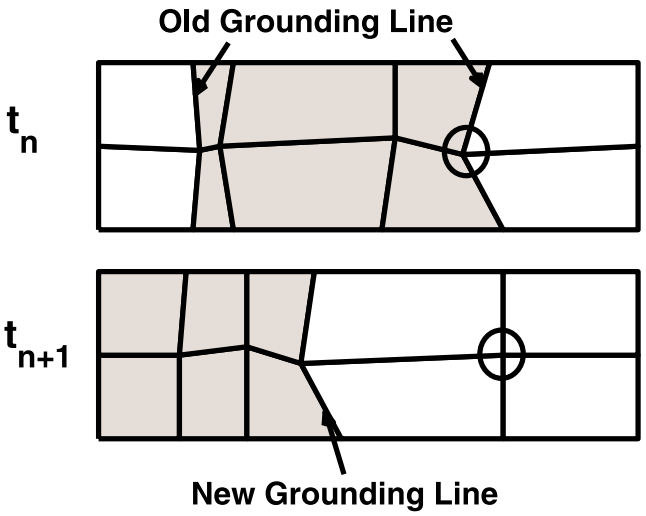

Figure 2. Visualization of moving mesh. (top) A hypothetical mesh at time t_n. (bottom) Mesh at the next time step. In both meshes the shaded cells comprise the grounded domain. Note that the circled node is the same node in both meshes, and it does not remain on the grounding line. Note also that the grounding line can easily change topology; at t_n it is not connected, but at t_{n+1} it is.

the new. A (slope-limiting) higher-order, mass conservative interpolative scheme is used. Our experience shows that the accuracy of this scheme is important to the results of the model, and that a low-order interpolation can make the solution excessively diffusive. The mesh moving scheme is similar to *Tan* [2007], although the form of the monitor function differs.

[31] Defining the mesh as a continuous mapping of the computational domain allows us to talk about uniformly increasing resolution even though resolution is not uniform. The mapping does not depend explicitly on the spacing of the computational mesh (the grid points in (ξ, η) coordinates); and if the solution h is not strongly dependent on this spacing, then increasing resolution uniformly on the computational mesh translates roughly to increasing resolution uniformly on the physical mesh.

[32] Note also that in our moving mesh scheme the grid points are not material points; they are not advected with velocity. Lastly, the equations (1, 2, 11) are solved on the physical mesh, not the computational one, and there is no change of variables involved. See Figure 2 for a visualization of the moving mesh scheme.

3.3.2. Adaptive Refinement

[33] Adaptive refinement, or h refinement, involves subdividing cells in regions where numerical error is high to improve accuracy, and merging cells in regions where error is low in order to save resources. How this error is assessed, however, depends highly on the equations being solved. Since in this problem stress gradients are expected to be highly localized, we use the jumps in strain rate at cell boundaries of the finite element solution to the diagnostic equations as a proxy for error. That is, for cell K,

$$\eta_K^2 = \int_{\partial K} \left(\left[\frac{\partial u}{\partial n}\right]^2 + \left[\frac{\partial v}{\partial n}\right]^2 \right) dl, \tag{23}$$

where $\frac{\partial(\cdot)}{\partial n}$ is differentiation in the direction normal to the cell boundary. Cells with the highest values of η are refined, while those with the lowest values are coarsened, with an overall constraint on the total number of cells. The algorithm by which cells are coarsened or refined, provided by the deal.ii library, ensures that a cell is bordered by cells that are neither more than one refinement level higher or lower than the cell. How many cells are refined and coarsened, as well as the maximum cell count, are user specified. In all adaptive refinement model runs, the cells contributing to the top 25% of the error are refined, and the cells contributing to the bottom 10% are coarsened. The refinement and coarsening takes place every 20–40 time steps, after which the thickness solution is interpolated to the new mesh.

[34] The form of η (up to a constant) was developed by *Kelly et al.* [1983] and is a generic estimator, i.e., it is not a true a posteriori error estimate of a finite element solution to (1, 2), but it has been found to be useful for adaptive refinement in a wide range of problems.

3.4. Grounding Line Movement

[35] The only way grounding line position feeds back in our model is in calculating basal shear stress and surface slope in (1, 2), so in general the grounding line is diagnosed from the floatation condition (8) just before solving for velocity. We can then represent the grounding line as lying along cell boundaries (i.e., every cell is either entirely grounded or entirely floating, depending on the average thickness and bed elevation in the cell), or interpolate the floatation condition between grid lines and allow cells to be partially grounded. In the latter case the integral arising from the $\vec{\tau}_b$ term in the weak form of (4) can be evaluated over partial cells by iterated quadrature. For our interpolation of the grounding line, we borrow from *Pattyn et al.* [2006] by taking the location of the grounding line to be given implicitly by

$$-\frac{\rho_w R}{\rho_i h} = 1. \tag{24}$$

where the left-hand side is defined bilinearly in each cell. It should be noted that this is just an interpolation of basal stress, not subgrid stress resolution: no additional degrees of freedom are used in the numerical representations of thickness and velocity. If there are scales in velocity or thickness that cannot be resolved by the mesh, subgrid grounding line interpolation will not remedy this. An advantage of interpolating the grounding line is that sudden changes in basal stress over large areas (relative to length scales of relevant quantities) are avoided. We use grounding line interpolation when using adaptive refinement but not when using a moving mesh (although experience with 1-D models suggests that grounding line interpolation would not affect the results of the moving mesh model). Both modes of grounding line movement allow for various topologies and topological changes of the grounding line, such as multiple grounded regions forming or becoming connected.

[36] Since the moving mesh scheme adapts the mesh based on thickness h while adaptive refinement depends on velocity u and v, the algorithms differ slightly between the modes of mesh adaption. Still, they are presented here

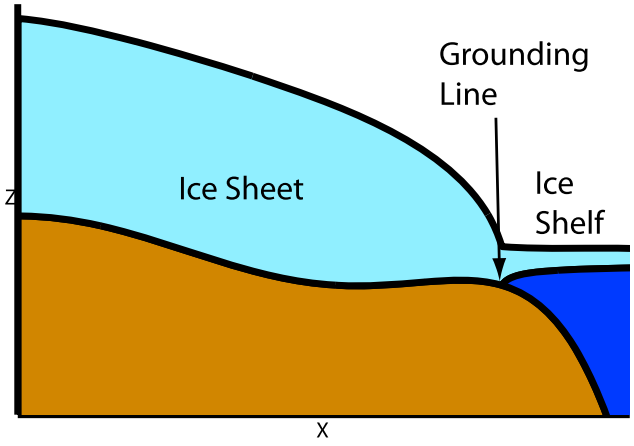

Figure 3. MISMIP experiment 3a: 1-D marine ice sheet over bedrock with sill.

together, where steps specific to mesh adaption are indicated. Note that the step labeled "adaptive refinement" is not necessarily executed every time step.

[37] 1. Piecewise constant thickness interpolated to continuous, piecewise bilinear function in order to force diagnostic equations.

[38] 2. Diagnostic equations solved for velocity with h held unchanged.

[39] 3. Mesh is refined and h interpolated to new mesh, then velocity found again (adaptive refinement).

[40] 4. Thickness evolved through continuity equation.

[41] 5. Mesh is moved and h interpolated to new mesh (moving mesh).

[42] 6. Floating domain found from floatation condition.

[43] 7. Repeat.

[44] Note there are three kinds of "interpolation" referred to in this chapter, and they are not to be confused with one another. One is the interpolation of the piecewise constant thickness to a continuous, piecewise bilinear function in order to solve for velocities. The second is the interpolation of the piecewise constant thickness on one mesh to a piecewise constant thickness on another mesh associated with mesh adaption. The third is the interpolation of the grounding line. The model code is written in C++ and uses the deal.ii adaptive finite element library (http://dealii.org).

4. 1-D Dynamics and Experiments

4.1. Steady States and Stability: MISMIP Experiments

[45] As described in section 1, *Weertman* [1974] predicts that two-dimensional marine ice sheets (i.e., with a single horizontal dimension and therefore described by a one-dimensional version of our depth-integrated model) should have well-defined, discrete equilibria whose stability is dictated by the slope of the ice sheet bed at the grounding line: steady grounding line positions on downward-sloping beds should be stable according to Weertman, and the grounding line should return to its original position after a perturbation to the ice sheet geometry, while steady grounding lines on upward-sloping beds are unstable and will irreversibly evolve away from their original position if perturbed.

[46] Weertman's argument hinges on the idea that grounding line mass flux increases with bed depth at the grounding line, since such a relationship is necessary for a slight grounding line advance to yield a negative mass balance for the grounded sheet on a downsloping bed, and a positive mass balance for a sheet on a foredeepened bed (and vice versa for a slight retreat). However, his theory is based on a relatively crude way of coupling sheet and shelf flows, and has been called into question as a result [*Hindmarsh*, 1996]. However, the recent results of *Schoof* [2007a, 2007b] have not only confirmed Weertman's qualitative results, but also put them on a much more quantitative footing. (It is worth mentioning that the quasi-analytical results of *Schoof* [2007a] are for an unbuttressed system. Schoof's boundary layer theory is not a suitable substitute for resolving the grounding line in the presence of buttressing.)

[47] These results form the basis of the Marine Ice Sheet Model Intercomparison Project (MISMIP; http://homepages.ulb.ac.be/~fpattyn/mismip/), which we use to test a 1-D version of our model. We discuss only Experiment 3a of the MISMIP series of experiments here, because it involves a bed with both upsloping and downsloping portions and provides a test not only of model agreement with Schoof's asymptotic results, but also lets us test whether stable steady states are indeed observed only on downsloping beds.

[48] In this experiment, an ice sheet is grown from zero thickness over a bedrock with a sill, as in Figure 3. All material parameters are spatially uniform, and are furthermore held constant over time with the exception of the fluidity parameter A in Glen's law. At prescribed intervals of 15–30 ka, A is changed from one constant value to another. Initially, A is decreased in several steps, and then increased again back to its original value, corresponding to first cooling and then warming of the ice. As A changes, the ice sheet successively adopts bigger steady state configurations during cooling, and subsequently retreats to small equilibrium shapes during warming. The objective of the experiment is threefold. First, Schoof's theory predicts the positions of steady states, and the experiment tests whether these are reproduced by the model. Secondly, some of the values of A in the experimental sequence correspond to more than one equilibrium shape, some of which are unstable, and the experiment tests whether the model captures these multiple equilibria, and whether it relaxes only to those predicted to be stable. Lastly, for those values of A for which Schoof's theory predicts only a single equilibrium, the experiment test whether the model reproduces this equilibrium in both advance and retreat, i.e., whether the grounding line shape returns to the original shape when A has first been decreased and then increased again to its original value.

[49] The MISMIP experiments are designed for ice sheet models with a single horizontal dimension, but a numerical model that solves the shelfy stream equations (1, 2, 11) can be reduced to this case by requiring that all data functions and dependent variables depend only on one of the spatial variables in these equations (in our case, x).

[50] The values of μ_1 and μ_2 in (21) and (22) were chosen as follows. An approximate measure of the nondimensional transition zone width is given by [*Schoof*, 2007a]

$$l_{bl} = \varepsilon^{\frac{n(m+2)}{n+m+3}}$$

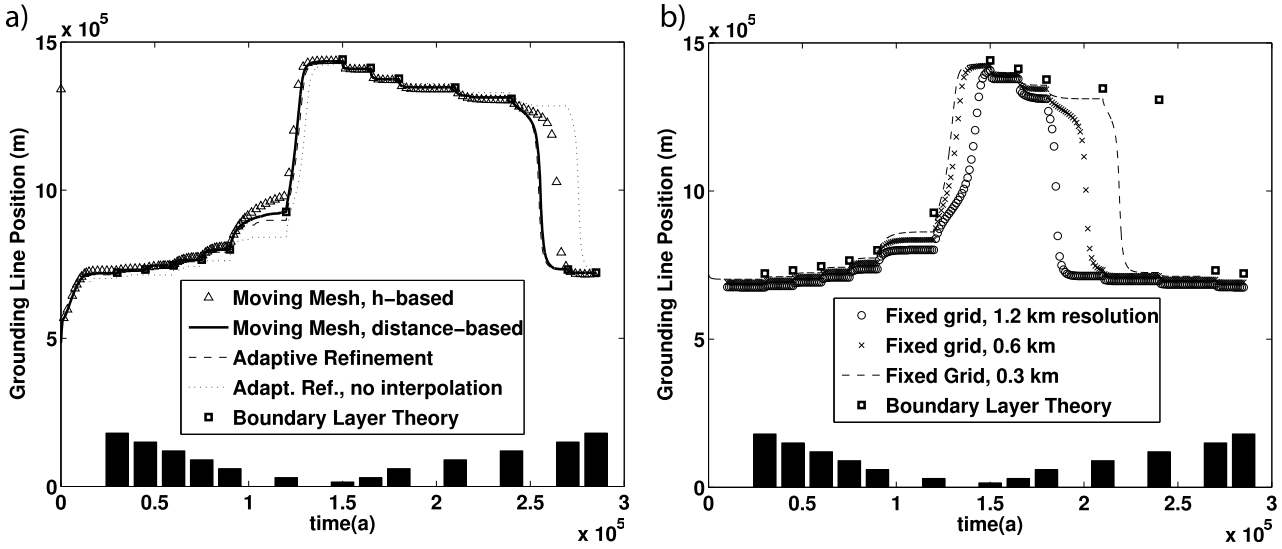

Figure 4. MISMIP experiment 3a: grounding line versus time. Squares represent the steady states predicted by the boundary layer theory. Bars show relative magnitude of Glen's Law constant A for time interval. (a) Moving mesh model and the adaptive refinement model. Solid line and triangles correspond to choices (21) and (22) of the monitor function ω, respectively. (b) Results without mesh adaption.

where ε is the same as in (12). (Note ε changes with A.) It was found that the choices $\mu_1 = .05 l_{bl}$, $\mu_2 = 10\mu_1$ gave a mesh with minimum spacing $\sim 0.2 l_{bl}$ when using a mesh with the smallest number of grid points considered. When using (22), the values $\mu_1 = 500$, $\mu_2 = 250$ seemed to give comparable resolution. All 2-D moving mesh simulations used (22) with these parameter values.

[51] Figure 4 shows results of MISMIP experiment 3a in the form of grounding line position over time. Adaptive mesh results are given in Figure 4a. Two sets of moving mesh results are shown, one where the distance-based monitor function given by (21) was used (solid line) and one where the thickness-based monitor function given by (22) was used (triangles). Adaptive refinement results with grounding line interpolation (dashed line) are shown as well. The steady states predicted by Schoof's asymptotic matching theory are shown too, for comparison. Relative magnitudes of A are indicated by vertical bars. The adaptive refinement with interpolation and moving mesh with monitor function (21) agree with each other and with the asymptotic matching theory to within a few kilometers. The moving mesh with monitor function (22) is somewhat worse; it seems that the asymmetry of h around the grounding line leads to a mesh that is not ideal for the problem. Still, the performance is much better than that of a uniform mesh with many more grid points (see discussion of Figure 4b).

[52] In Figure 4a we also show results for the adaptive refinement method without grounding line interpolation (dotted line). These do not agree as well with the other results of adaptive refinement with grounding line interpolation, or with the moving mesh or asymptotic matching results. Importantly, the degree of refinement in these runs without grounding line interpolation was the same as in the runs with grounding line interpolation. This suggests that numerical inconsistencies cannot be attributed to under-resolution of stress gradients in the grounding line transition zone alone, which were suggested by *Schoof* [2007b] as the cause of the inconsistent results obtained in previous work [e.g., *Vieli and Payne*, 2005]. There may also be a "kinematic" problem: velocity field, while known accurately, does not lead to the correct switching of cells between grounded and floating because such switching requires an average thinning or thickening over a spread-out area (the area of the cell). This may be attributable to the large thickness gradients that prevail near the grounding line, which can lead to one end of a grid cell being significantly above flotation while the other is significantly below. A method that does not interpolate the grounding line then has to treat such a cell as being either completely afloat or completely grounded, with yields a discontinuous switch in basal friction that feeds back into the velocity field.

[53] In Figure 4b results of MISMIP experiment 3a are also shown for fixed, uniform meshes with approximately 1.2, 0.6 and 0.3 km resolution, respectively. As in the adaptive refinement simulation, grounding line interpolation (see 3.4 above) was used. Their agreement with each other and with the boundary layer theory is worse than that of the mesh adaptive results. For comparison, the adaptive mesh method developed meshes with less than 100 m resolution near the grounding line, while using the same number of grid points as a fixed mesh simulation with $\sim$4 km resolution.

[54] Several important results can be inferred from our 1-D experiments. First, the model seems to be numerically convergent. In the fixed grid simulations the agreement with the boundary layer theory improved as resolution increased. (In the instances when the fixed grid models did not find steady state solutions on the seaward side of the sill in Figure 3, it was because the grounding line was too close to the back of the sill, although this too improved with resolution.) We see that our model, which is inherently designed to be applicable to two horizontal dimensions, simulates grounding line movement in one horizontal dimension in good agreement with theory. Second, this good agreement with the asymptotic matching theory and of our

different mesh refinement methods with each other show that convergence can be achieved with relatively low computational cost. This is perhaps not crucial for the 1-D simulations above, where very high-resolution runs can be done on laptop computers, but for a comparable 2-D domain it would be very difficult to achieve resolution below a kilometer with uniform meshes. Third, the adaptive refinement simulations show an improvement when grounding line interpolation is utilized, even though all other numerical parameters are held constant. The above fixed mesh simulations were also run without making use of grounding line interpolation, and the results were far worse: while the initial grounding line advance up to 150 ka was similar to that shown in Figure 4b, there was almost no subsequent retreat (not shown). This implies that the difficulties with grounding line migration are not solely because of failure to resolve the stress transition.

4.2. Comparison With Previous Numerical Solution Attempts: Eulerian Versus ALE Methods

[55] In previous attempts to simulate ice sheets with one horizontal dimension, significant discrepancies were found between models using different methods of treating grounding line migration. *Vieli and Payne* [2005] examined two such methods, which they termed ''fixed grid'' and ''stretched grid'' (the latter is not to be confused with our term moving mesh). In their fixed grid model the grounding line was found from the floatation condition after evolving thickness, and it was constrained to lie on cell boundaries. By contrast, their stretched grid method mapped the grounded portion of the physical domain onto the unit interval in their computational domain, and employed an evolution equation grounding line position based on differentiating the flotation condition $\rho\, h = -\rho_w R$ as in the work of *Hindmarsh* [1996]. In standard nomenclature, the stretched grid method can be considered Arbitrary Lagrangian-Eulerian (ALE) type, as opposed to their fixed grid, which is purely Eulerian.

[56] *Vieli and Payne* [2005] found that their stretched grid model predicts grounding line advance as well as retreat in response to perturbations and that the response to small perturbations was reversible (although the effect of larger perturbations was not completely reversible). In the fixed grid method, on the other hand, the grounding line would not retreat in response to perturbations, and perturbations that caused it to advance were irreversible. Also, response to perturbations depended quantitatively on grid spacing in the fixed grid method.

[57] These results suggest that *Vieli and Payne*'s [2005] fixed grid method cannot capture grounding line dynamics accurately, and raises two questions. First, what aspect of the fixed grid method prevents grounding line retreat, and secondly, is there a generic problem with applying Eulerian methods to track grounding line motion? The small length scales predicted by Schoof's analysis suggest insufficient resolution as a possible reason for the inconsistencies in Vieli and Payne's experiments. In addition, the superior performance of the ALE method also suggests that the inability of the fixed grid method to track grounding line motion on distance below the grid scale could play a role, and this is relevant to Eulerian methods in general.

[58] However, even accepting that ALE methods may be preferable in 1-D cases, they do not generalize easily to 2-D simulations. They involve changes of coordinates that have the potential to become very poorly conditioned and have difficulties with changing grounding line topologies. They also require prognostic equations for grounding line migration that would be difficult to evaluate. They also have difficulties with changing grounding line topologies. In two horizontal dimensions, a Eulerian approach is therefore the realistic choice, and is adopted here: although our mesh points may change physical location, the diagnostic and continuity equations are always solved in a Eulerian frame. One of the important results of our 1-D experiments above has therefore been that our method, which is inherently Eulerian regardless of the mesh refinement method (moving mesh or adaptive refinement), does not have the shortcomings of *Vieli and Payne*'s [2005] fixed grid method. By increasing resolution near the grounding line, and by including the grounding line interpolation of *Pattyn et al.* [2006] in our adaptive refinement runs to allow for subgrid grounding line movement, we have obtained results that are both internally consistent between runs with different grid spacings and with different mesh refinement methods, and that are in agreement with the quasi-analytical results of *Schoof* [2007b].

[59] It should be noted at this point that our goal in demonstrating the robustness of our model is to bolster confidence that our numerical model is solving the PDEs we have charged it so solve. We cannot prove convergence of our discretized solution to the (or a) weak solution of our PDE system, since we cannot use the Lax equivalence theorem [*Lax and Richtmeyer*, 1956] (our system is nonlinear) or the Lax-Wendroff theorem (which applies to pure conservation laws), although the convergence of our solver for the diagnostic equations (1, 2) can be shown using the methods of *Reist* [2005] and *Schoof* [2009]. However, the fact that our model agrees with the quasi-analytical steady state solution in the MISMIP experiment, and that our results are robust to changes in numerical details, gives us confidence that our model is performing correctly.

5. 2-D Experiments

[60] As described in the introduction, the presence of lateral shear in ice shelves may have a significant effect on the dynamics of marine ice sheets with ice shelves that are confined to embayments, or which contain grounded ice rises. To address this, we test our model in 2-D settings, with variations in velocity and thickness in both horizontal coordinates. First, we test model performance to ensure that the positive results obtained above translate to the 2-D case. Subsequently, we investigate how buttressing in an ice shelf affects the qualitative dynamics of a marine ice sheets (in terms of the location and stability of its steady states) and attempt to identify the controlling physical parameters in buttressing.

5.1. Downsloping Bed Experiments

5.1.1. Steady States

[61] By contrast with the 1-D case, there is no quasi-analytical steady state solution or other benchmark to compare our results with. To test model performance, we

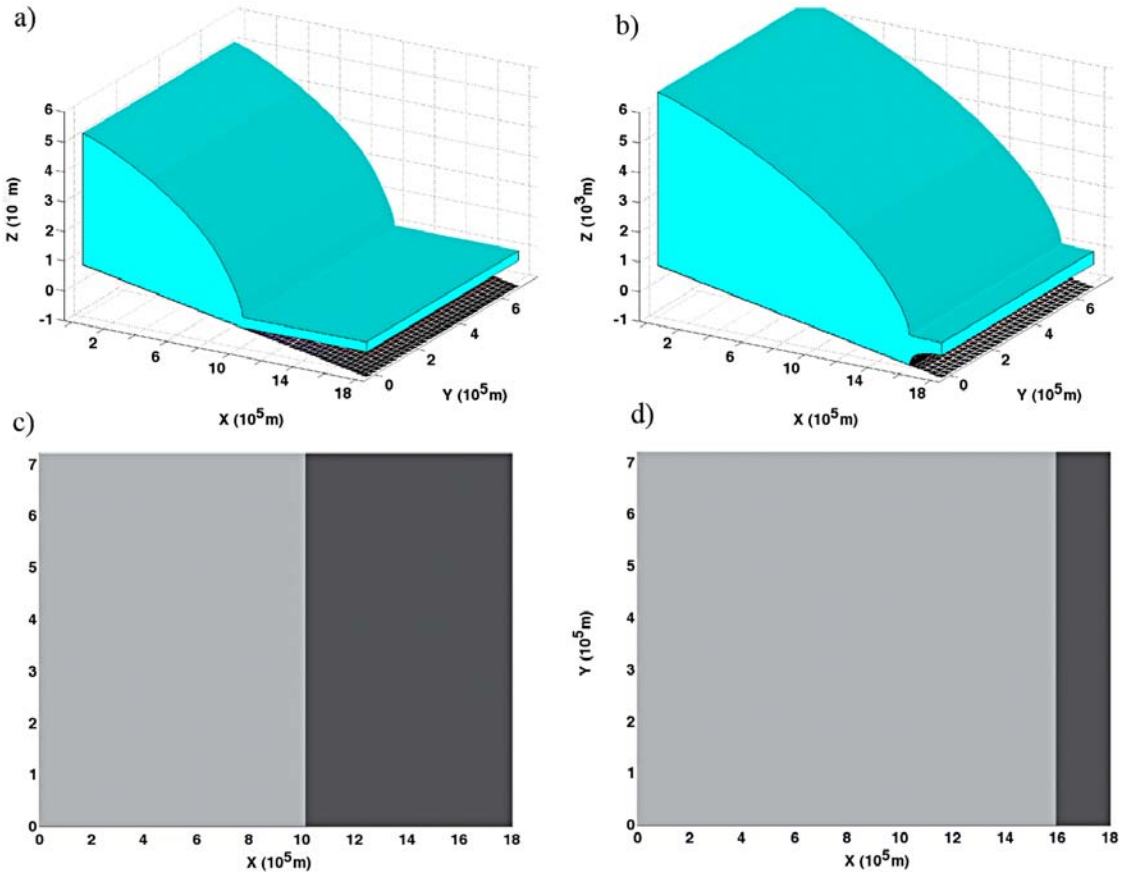

Figure 5. Downsloping bed experiments with moving mesh: differing initial conditions. (a) Short-stream initial condition: side view of marine ice sheet. Gap below ice shelf is ocean cavity. (b) Long-stream initial condition. Note difference in grounding line position and divide thickness. (c) Top-down view of short-stream initial condition (dark portion is floating ice). (d) Top-down view of long-stream initial condition.

therefore check our results for internal consistency: do runs with different mesh refinements and number of grid points agree with one another? Moreover, in the case of a wide ice shelf in which little lateral shearing occurs, we expect to recover at least the qualitative dynamics of the 1-D case, which provides a further check on our model.

[62] Our first set of experiments was carried out for a downsloping bed of the form

$$R(x,y) = 720\ \text{m} - 1.038 \times 10^{-3}\ x, \tag{25}$$

with the end of the shelf fixed at $x = 1.8 \times 10^6$ m. The lateral boundaries of the domain are at $y = 0$ m and $y = 0.72 \times 10^6$ m, where we prescribe no-slip boundary conditions. We assume an ice divide at $x = 0$ m, and thus velocities are zero at this boundary. As material parameters, we used $\rho = 900$ kg, $\rho_w = 1000$ kg, $C = 7.6 \times 10^6$ Pa $(\text{m}^{-1}\text{s})^{1/3}$, $m = 1/3$, and $A = 0.8 \times 10^{-25}$ $\text{Pa}^{-3}\text{s}^{-1}$ which, through the thermal dependence of A [*Paterson*, 2001], corresponds to an ice temperature of -25°C. We started our runs with two different sets of initial conditions, one with a grounding line close to the ice shelf front, and one with a grounding line far from the front. These will be referred to as the "long-stream" and "short-stream" initial condition, respectively. The initial profiles are y-independent and differ only in the choice of initial grounding line position x_g. They are defined as follows (see also Figure 5):

$$h(x,y)|_{t=0} = \begin{cases} \left[h_g^{m+2} + \dfrac{m+2}{m+1}\dfrac{Ca^m}{\rho g}\left(x_g^{m+1} - x^{m+1}\right)\right]^{\frac{1}{m+2}} & x < x_g \\ \left[\dfrac{c_A}{a} - \dfrac{u_g^{n+1}\left(\frac{c_A}{a}h_g^{n+1} - 1\right)}{\left[a(x - x_g) + u_g h_g\right]^{n+1}}\right]^{-\frac{1}{n+1}} & x \geq x_g. \end{cases} \tag{26}$$

Here

$$c_A = \left(\frac{\rho g(\rho_w - \rho)}{4\rho_w}\right)A$$

$$h_g = \frac{\rho_w}{\rho}|R(x_g)|, \qquad u_g = a x_g,$$

and a is the spatially uniform accumulation rate (equal to 0.3 ma^{-1}). h_g can be interpreted as the floatation thickness at x_g corresponding to (25), and u_g as the velocity required for the sheet to be in equilibrium for a given x_g. The $x < x_g$ case of (26) is the equilibrium profile of the grounded

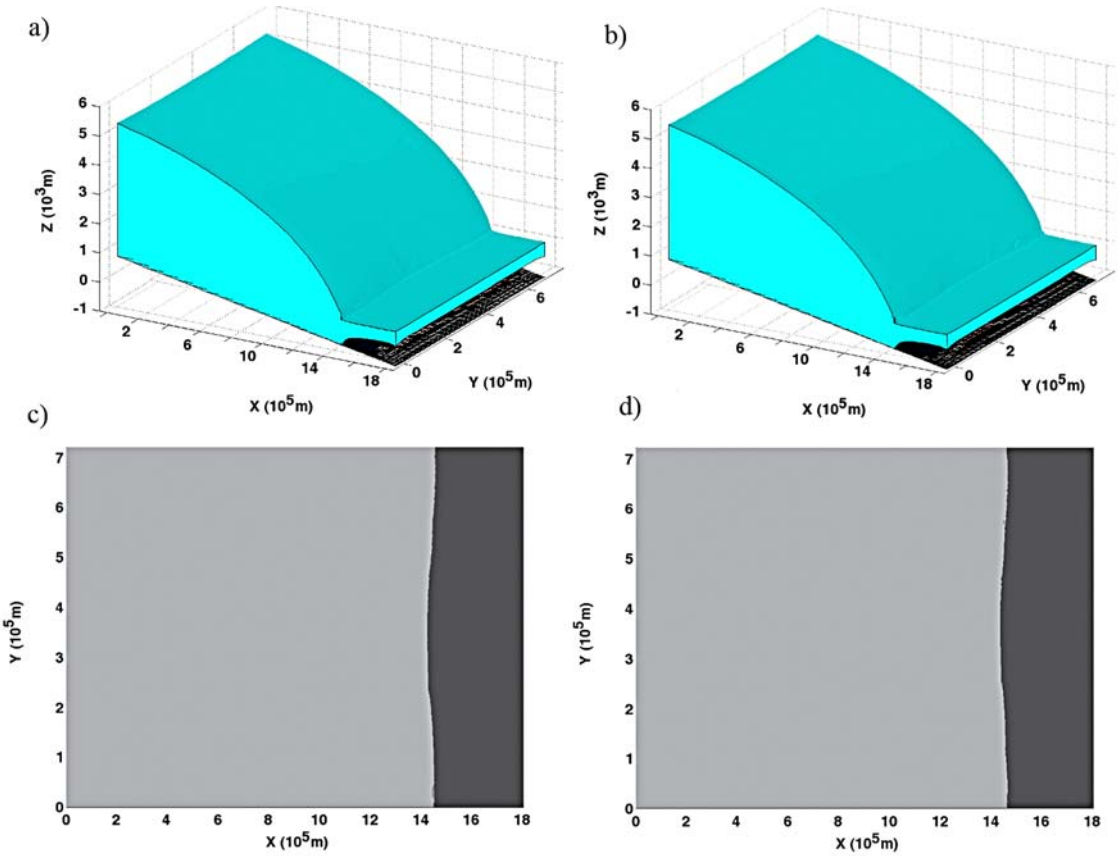

Figure 6. Downsloping bed experiments with moving mesh: steady states. (a) Steady state evolved to from short-stream initial condition, 12.5 ka. (b) Steady state evolved to from long-stream initial condition. (c) Top-down view of Figure 6a (dark portion is floating ice). (d) Top-down view of Figure 6b.

portion of a 1-D sheet with uniform accumulation and grounding line x_g, ignoring longitudinal stresses [*Schoof*, 2007a]. The $x \geq x_g$ case (floating case) is the equilibrium profile of a 1-D ice shelf with uniform accumulation and grounding line x_g [*Van der Veen*, 1999].

[63] Figure 6 shows the results of the experiment for a moving mesh simulation with 30 × 60 resolution, which would give grid spacing of about 30 km for a uniformly spaced fixed grid. Figures 6a and 6c correspond to the short-stream initial condition, and Figures 6b and 6d correspond to the long-stream initial condition. As can be seen the two initial conditions evolve to nearly identical steady states, suggesting that there is a unique steady state.

[64] It is fairly straightforward to evaluate numerical convergence with our moving mesh model. Figure 7 shows such an evaluation for the short-stream experiment. Figure 7a is the same steady state as in Figures 6c and 7b is the corresponding mesh. Compare these with Figures 7c and 7d, the equivalents for a mesh with 50 × 100 grid points. The steady states are very similar in appearance, and the finer mesh looks like a uniformly resolved version of the coarser mesh, as predicted. The shortest distance between grid lines in the coarser mesh is about 700 m.

[65] The experiments were repeated with the adaptive refinement method, with a maximum cell constraint of 8000 cells, and the steady state results are shown in Figure 8. The steady state found by integrating from the short-stream initial condition was similar to that found by the moving mesh counterpart. However, the sheet beginning from the long-stream initial condition retreated to an apparent steady state that did not agree with the short-stream steady state as well. While the grounding line did retreat significantly from its initial condition (about 150 km), it still ended up about 50 km seaward of that in the moving mesh simulations. Also, examination shows that grounding line shape differs as well: in the moving mesh results, the grounding line flattens out near the sidewalls, while for adaptive refinement the grounding line has more of a parabolic shape.

[66] In the adaptive refinement runs, the most highly resolved cells in the transition zone had a diameter of 2.25 km, on the same order as but still larger than in the moving mesh simulations. By contrast, in the MISMIP experiments above, the most highly resolved cells in the moving mesh and adaptive refinement simulations had nearly the same diameters, suggesting that adaptive refinement may still have underresolved the transition zone in the 2-D downsloping bed experiments. Lower resolution in the transition zone was likely a result of the details of the adaptive refinement scheme, which refines against a constraint on the maximum number of cells. Because of the no-slip condition at the shear margins, those regions demanded higher resolution (and more cells) at the cost of resolution in the transition zone.

[67] Resolution near the shear margins may also explain the differences in grounding line shape. Figures 7b and 7d both show that when the moving mesh is used, the cross-

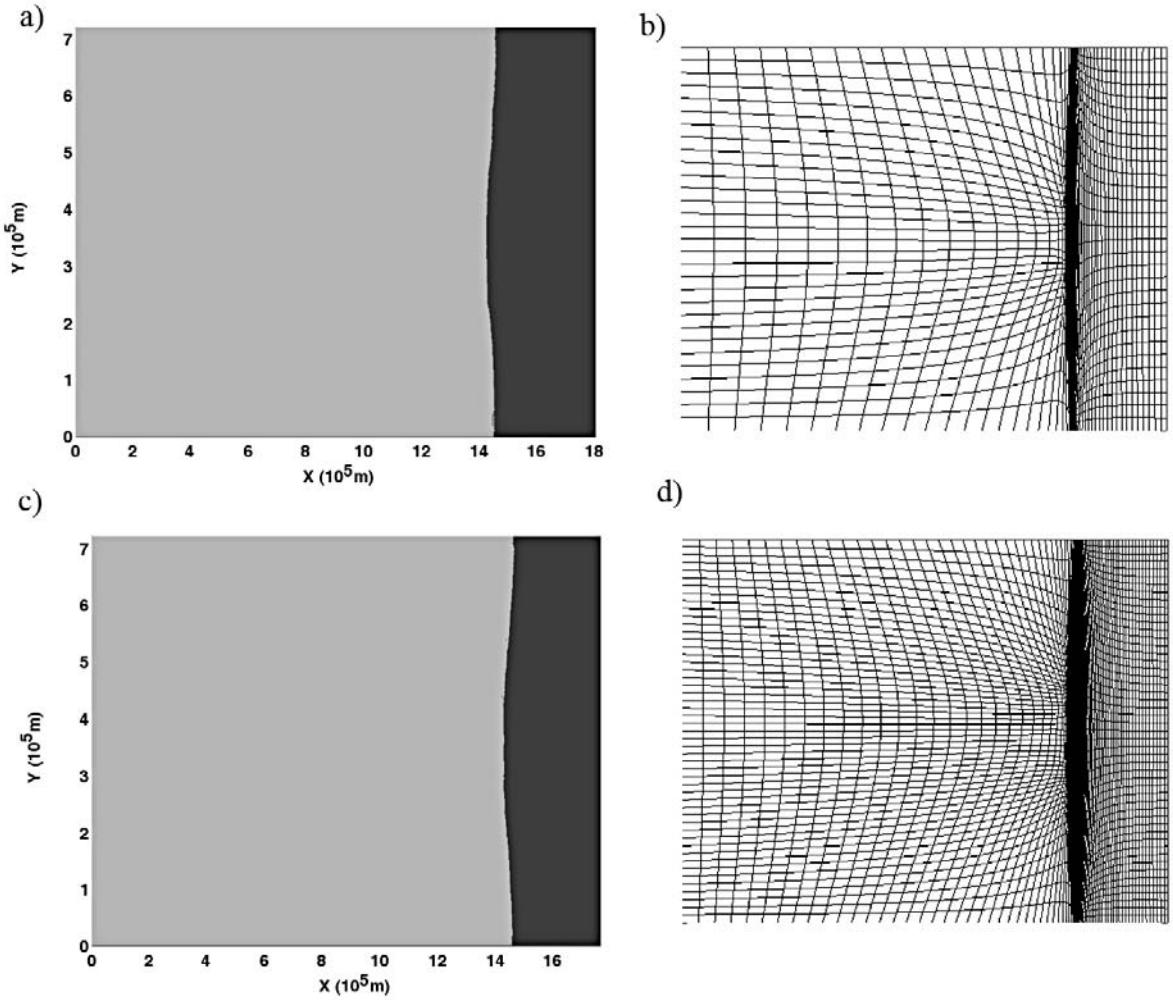

Figure 7. Downsloping bed experiments with moving mesh: sensitivity to mesh size. (a) Steady state evolved to from short-stream initial condition, 30 × 60 grid. (b) Mesh corresponding to steady state from short-stream initial condition, 30 × 60 grid., (c) Steady state evolved to from short-stream initial condition, 50 × 100 grid. (d) Mesh corresponding to steady state from short-stream initial condition, 50 × 100 grid.

flow diameter of grid cells differs greatly across the grounding line, with the cells on the grounded side being much wider. Therefore, the no-slip condition is felt further from the wall on the grounded side, and velocities are lower. The flux difference leads to increased thinning near the margin, and as a result the grounding line is slightly more recessed in that region than it should be. It is likely, though, that with the moderate channel width in these experiments, the margins play a smaller dynamic role than longitudinal stresses, and therefore their underresolution, despite localized error, did not affect the overall ice sheet evolution. Therefore, the moving mesh, which focused resolution in the transition zone, produced better results for these experiments.

[68] Performance of the adaptive refinement method without grounding line interpolation was even worse (echoing the results of the 1-D experiments). The short-stream initial condition still evolved to the same steady state, but in the long-stream simulation the grounding line retreated less than 50 km. Again, this is remarkable because the resolution of the runs without grounding line interpolation yield the same cell size near the grounding line as the corresponding runs with interpolation. By contrast with the 1-D experiments above, our 2-D runs were restricted to lower resolutions due to computational cost, and the effect of having to treat the now much larger grid cells as being either completely afloat or completely grounded is even more noticeable.

[69] We give some idea of the cost of a uniform mesh with comparative along-flow resolution, focusing on the linear solve in the iterative solution for velocity, which is the most resource-intensive part of the simulation (although for meshes with less than ∼5,000 cells the assembly of the linear system takes an amount of time comparable with that of its solution). Results are given for moving mesh and adaptive refinement simulations, as well as fixed (uniform) meshes, and are summarized in Table 2. In each case the physical domain dimensions were 1800 × 720 km, and each nonlinear velocity solve began with an initial guess of $\vec{u} \equiv 0$ and took 42 iterations (with a single linear solve each iteration) to reach desired tolerance. Dimensions of the fixed mesh were chosen so that along- and cross-flow

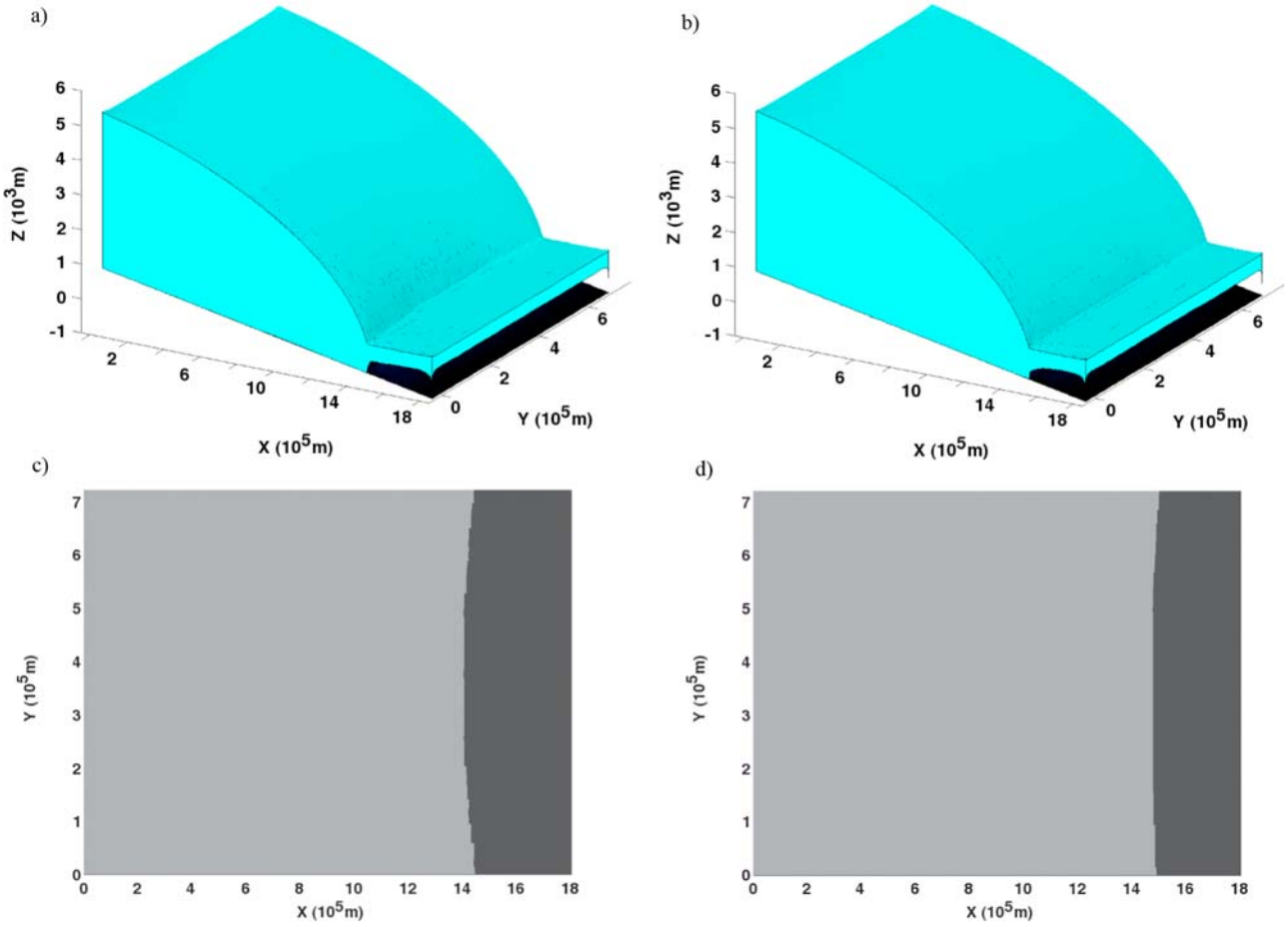

Figure 8. Downsloping bed experiments with adaptive refinement: steady states. (a) Steady state evolved to from short-stream initial condition, 12.5 ka. (b) Steady state evolved to from long-stream initial condition. (c) Top-down view Figure 8a (dark portion is floating ice). (d) Top-down view of Figure 8b.

resolution near the grounding line was comparable with the moving mesh and adaptive refinement simulations, respectively. In the former case (see Table 2), poor performance could be because the PETSc conjugate gradient iteration failed with a block Jacobi preconditioner, whereupon a Jacobi preconditioner was used.

5.1.2. Response to Perturbations

[70] Our results above have already suggested that, for a given set of physical parameters and a fixed ice shelf front position, the ice sheet with a downsloping bed settles to a unique equilibrium regardless of initial conditions. In 1-D, this is one of *Weertman*'s [1974] original predictions for a downsloping bed, and is confirmed by *Schoof* [2007a] and by our MISMIP runs above. However, as shown by *Vieli and Payne* [2005], numerical models in 1-D may or may not reproduce this behavior depending on the method of tracking the grounding line that they employ, and crucially, depending on resolution near the grounding line.

[71] In two horizontal dimensions, we have no equivalent to Weertman's or Schoof's results, but our numerical results above suggest that both observations translate from 1-D to 2-D: There is apparently a unique equilibrium shape even in two dimensions, but that not all numerical solutions will reproduce this behavior (notably the adaptive meshing results without grounding line interpolation above). Here, we investigate this basic question further: does a marine ice sheet have well-defined, discrete equilibria for a given set of material and geometrical parameters and physical forcings?

[72] However, instead of starting simulations from different initial conditions, we follow *Vieli and Payne* [2005] and

Table 2. Comparison of Computational Cost of Mesh Adaption Schemes With Uniform Meshes[a]

Mesh Adaption Scheme	Grid Size	Minimum Along-Flow Resolution (km)	Average Linear Solve Time (s)
Moving mesh	30 × 60 cells	1	0.03
None	30 × 1000 cells	1.8	3
Adaptive refinement	10,000 cells (maximum)	2.5	0.07
None	144 × 360 cells	5	2.5

[a]In the rows corresponding to a uniform mesh (denoted by "none"), mesh dimensions were chosen to have comparable resolution with that of the preceding row near the grounding line.

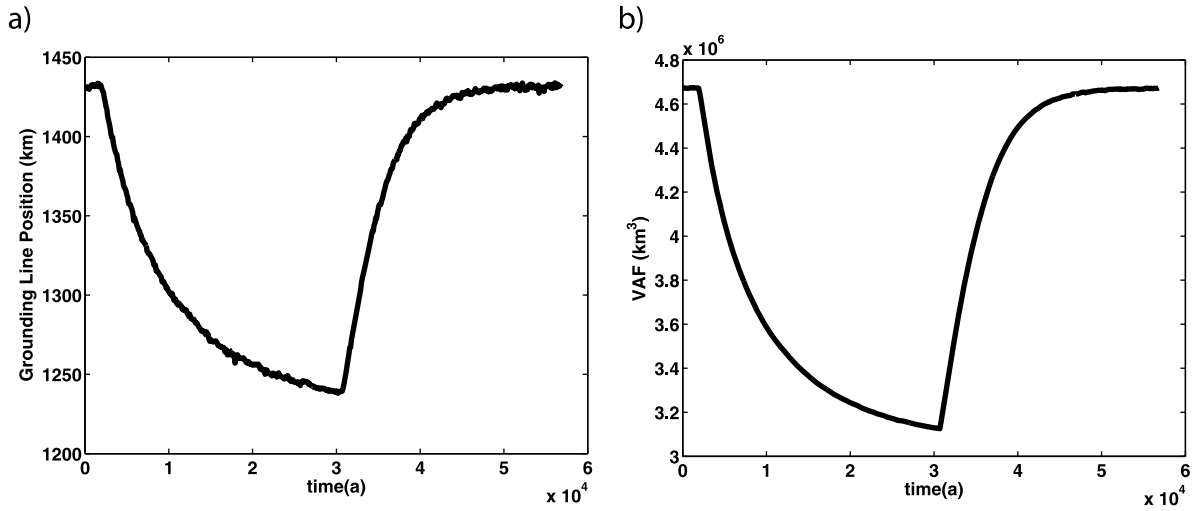

Figure 9. Response to step changes in accumulation. (a) Evolution of minimum grounding line position. (b) Evolution of volume above floatation (*VAF*).

subject an ice sheet that is already in an equilibrium shape to a step change in accumulation rate, and subsequently reverse this step change. In Figure 9 we show the response of our model to such an accumulation step change: accumulation (a) is decreased from 0.3 ma^{-1} to 0.06 ma^{-1} and the model is integrated until retreat has slowed appreciably. Then a is increased back to its initial value and the system is again allowed to reach a steady state. Figure 9a shows the position of the leftmost point of the grounding line (the point on the grounding line with the smallest x coordinate) as a function of time. Figure 9b shows the evolution of a different metric, volume above floatation (*VAF*), with is useful because it looks at the whole sheet instead of a single part and its evolution is smoother than that of grounding line position. Both curves show that the marine ice sheet returns back to its original steady state after the perturbation is removed. (The criterion for ending the simulation was assessment of a steady state by inspection, but results show that VAF varied by $\sim$7 km^3 over the final 5 ka, less than 1% of the total variation of the simulation.)

[73] We offer a heuristic explanation for why there is a single equilibrium shape for a given set of physical parameters. In the absence of buttressing, the grounding line has a unique stable steady configuration because mass flux through the grounding line can be computed as a function of ice thickness there, and the equilibrium balance between inland accumulation and flow through the grounding line leads to a unique steady state [*Weertman*, 1974; *Schoof*, 2007a]. In the presence of buttressing, this simple argument no longer holds because grounding line flux is no longer determined by ice thickness alone, but also by longitudinal stress at the grounding line (which is itself a function of ice thickness in the unbuttressed case).

[74] However, other effects being equal, the total lateral shear stress on the shelf increases with the length of the shelf, and leads to a corresponding decrease in longitudinal stress at the grounding line. If the introduction of lateral shearing leads to an altered equilibrium shape, we argue that it should again be stable. This is because a slight advance in the grounding line will lead to a shorter shelf and less buttressing, so the longitudinal stress at the grounding line should increase by at least as much as in the unbuttressed case. There are other effects associated with an advance of the grounding line, such as change in the velocity field and a slight increase in the thickness of the shelf near the grounding line (which leads to slightly increased buttressing) but we do not expect them to dominate. So in the regime of modest buttressing (i.e., shelf width comparable to shelf length) we expect a unique stable steady state over a downsloping bed. This is by no means a formal argument, but is supported by our numerical results above.

5.2. Buttressing Experiments

[75] A much more complicated scenario is that of a foredeepened bedrock. In 1-D, this admits no stable steady states [*Weertman*, 1974]: if there were an equilibrium configuration with its grounding line on the upward-sloping bed, then a retreat from that grounding line position would lead to greater mass flux through the grounding line, and hence accelerated retreat. However, the effect of lateral shearing in two dimensions could conceivably change the qualitative behavior of the system. With lateral shearing, longitudinal stress and hence ice flux at the grounding line are affected by changes in ice shelf geometry. Suppose that there is an equilibrium position with the grounding line positioned on the foredeepened bed in the presence of buttressing. A retreat in the grounding line will still lead to greater ice thickness at the grounding line, which tends to increase mass flux there. However, with a fixed ice shelf front it also corresponds to a longer ice shelf in which lateral shearing plays a stronger role, and this will tend to lower longitudinal stresses and hence mass flux. Which of these two competing effects will dominate is unclear; if the former, then Weertman's marine ice sheet instability will persist, while grounding lines on foredeepened slopes would be stabilized if the latter effect is more important.

[76] To test whether buttressing could lead to stabilization and to identify the controlling parameters, we ran our model with a foredeepened bedrock of the form

$$R(x,y;\alpha) = \begin{cases} -600\ \text{m} + \alpha(x - .96L_x) & x < .96L_x \\ -600\ \text{m} - 0.02(x - .96L_x) & x \geq 0.96L_x, \end{cases} \quad (27)$$

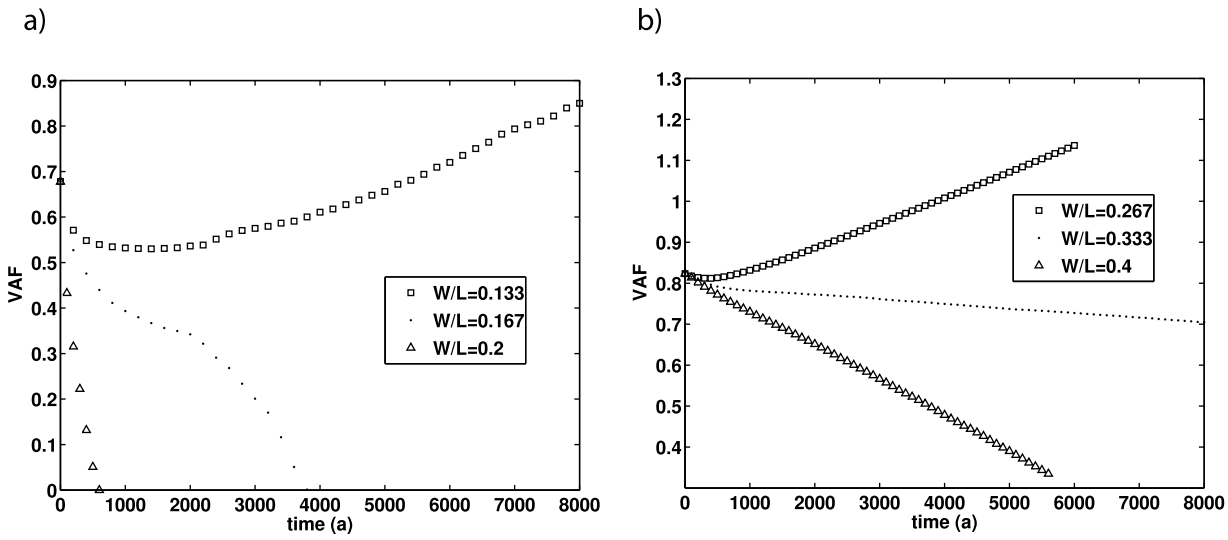

Figure 10. *VAF* over time for selected runs from the buttressing experiments. Width is increasing from top to bottom curves in both plots. (*VAF* is normalized due to differing channel widths.) *VAF* for different values of *W*/*L* over an (a) steep ($\alpha = 10^{-3}$) and (b) gentle ($\alpha = .25 \times 10^{-3}$) foredeepened bed.

where L_x is the length of the domain (equal to 1500 km unless otherwise specified) and α is the bottom slope. The sharp slope past $x = .96L_x$ signifies a continental shelf break. Similarly to the Downsloping bed experiments, $y = 0$ and $y = W$ were no-slip boundaries, where W, the channel width, was varied between simulations. Material parameters and accumulation rates were spatially uniform, and unless otherwise specified the accumulation rate a was equal to 0.3 ma^{-1}. It can be show by scaling as in section 2.1 that the behavior of such a system depends four dimensionless groups. In order to identify how the stabilizing effect of buttressing is controlled, we therefore vary four model parameters, namely, domain width (W), bedrock slope (α), Glen's law constant (A), and basal friction coefficient (C). Each model run was begun with an initial condition of the form (26), with $x_g = 700$ km.

[77] Rather than performing a full search of a section of four-dimensional parameter space, we first varied W and α while holding A and C constant at $A = 1.5 \times 10^{-25}\text{Pa}^{-3}\text{s}^{-1}$ (corresponding to a temperature of $-20°\text{C}$), $C = 7.6 \times 10^6$ Pa $(\text{m}^{-1}\text{s})^{1/3}$. Subsequently, we fixed $W = 600$ km, $\alpha = 0.5 \times 10^{-3}$ and varied A and C instead.

[78] With A and C fixed, bed slope was varied between 10^{-3} and 0.25×10^{-3}, values slightly lower those found in the WAIS, and W was varied between $0.1L_x$ and $0.67L_x$. Figure 10 plots *VAF* against time for several (W,α) pairs. The left plot shows results for decreasing values of W over a steep bed while the right shows the same over a bed with gentle slope. In all but one case, collapse of the ice sheet is observed from the prescribed initial configuration. Note that for a wide channel (triangles) the collapse occurs relatively quickly while for a narrower channel (circles) it is slower. For the narrowest domain, we instead see an advance, which is eventually halted by the continental shelf at the edge of the domain. Comparing the left and right plots, we see that collapse tends to happen more quickly for a steeper bed and that the collapse time scale seems to be more sensitive to changes in width for the steeper slope.

[79] Importantly, the results Figure 10 do not show a reversal of stability: no stable steady states appear on the foredeepened bed, and Weertman's instability appears to persist. Both the unstable collapse observed in most of the simulations and the advance predicted for the simulations with the narrowest domain are consistent with this, and the fixed initial conditions dictate for each set of parameter values whether advance or retreat is observed. This was also confirmed by redoing several of the simulations in Figure 10b with different initial conditions, which confirmed that the ice sheet would always collapse or advance to the edge of the domain, with small initial grounded domains favoring collapse and larger ones favoring advance.

[80] The results of the (W,α) parameter search are summarized in Figure 11. This is a contour plot in (W,α) space

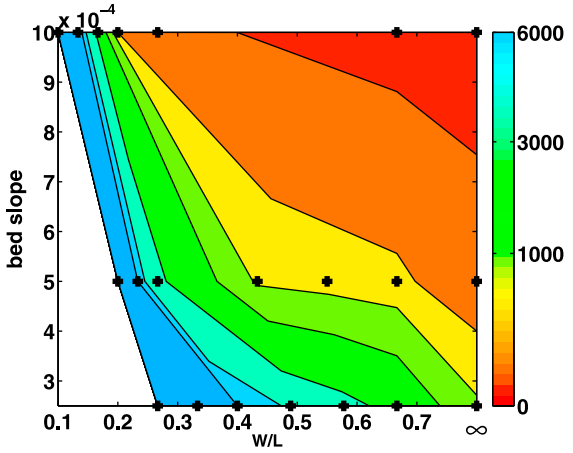

Figure 11. Results of buttressing experiments. Time from start to collapse (the time at which $VAF = 0.1 \times VAF_0$) denoted by contours. Actual data points are denoted by crosses. The leftmost filled contour indicates very slow retreat or unstable advance.

of the time that it took for the sheet to go from our initial condition to collapse, defined as *VAF* reaching 10% of its original value. The leftmost filled contour is where the sheet either took over 6ka to collapse (a long time, even on glacial time scales) or advanced to the continental shelf, and the right hand border shows the extreme case of an infinitely wide channel (the 1-D case). Again we see that collapse is much faster on a steeper bed, and that on such a bed the transients are much more sensitive to the width of the channel. If we interpret the change in time to collapse (or the transition from collapse to advance) as a change in position of an unstable steady point, this change is apparently more sensitive to channel width on a steeper slope.

[81] After exploring the effect of width and slope, we fixed W and α and allowed C and A to vary. The basal stress coefficient C was varied between 5×10^6 and 14×10^6 Pa $(\mathrm{m}^{-1}\mathrm{s})^{1/3}$, and the Glen's Law constant was varied between.6 $\times$ 10^{-25} and 3.6 $\times$ $10^{-25}\mathrm{Pa}^{-3}\mathrm{s}^{-1}$, corresponding to temperatures between -28°C and -12°C. The results were qualitatively the same as for the case of varying W and α, with either collapse or advance to the edge of the domain occurring in each case. Briefly, collapse tended to happen faster with a smaller basal stress coefficient, which is to be expected because this increases flow velocities. A larger value of A (i.e., a higher temperature) also leads to a faster collapse, while at the largest values of A, the ice sheet with the prescribed initial condition advanced to the edge of the domain instead of collapsing. Again, this was expected because higher A leads to higher strain rates and velocities in the shelf and transition zone, and thus greater flux at the grounding line, and has the effect of weakening the buttressing, with the opposite occurring for low A.

[82] While we did not find that buttressing effects are enough to overcome the inherent instability of a marine ice sheet in the parameter space described above, other authors have reported stabilization of marine ice sheets by buttressing in similar models. Using a quasi 2-D model, *Dupont and Alley* [2005] reported stabilization of a marine ice sheet on a foredeepened bed. To determine whether our model reproduced this behavior, we performed an experiment using parameters similar to their study.

[83] In the model of Dupont and Alley, the bed slope was steeper, the domain smaller, and the basal traction weaker than in our Buttressing experiments detailed above, and so we adopted these new parameters. Our simulation differed in two other ways: our boundary conditions at the $x = 0$ boundary were different, and we resolved the transverse direction and buttressing effects, while in the Dupont and Alley study buttressing was parameterized.

[84] In the Dupont and Alley model, the $x = 0$ boundary condition(s) consisted of velocity and thickness being held constant at u_0 and h_0, respectively, which was different than our assertion of an ice divide (zero velocity, unconstrained thickness) at the $x = 0$ boundary. Instead of adopting different boundary conditions, we extended the $x = 0$ boundary farther away from the ice shelf front and chose a uniform accumulation. The Dupont and Alley model asserted a flux of $q_0 = h_0 u_0$ at a certain distance inland from the ice shelf front. We chose our accumulation rate such that, in a steady state, the marine ice sheet would have a mass flux q_0 at the same physical location. And again, in our simulation the boundaries at $y = 0$, $y = W$ were no-slip boundaries.

[85] In our simulation we chose $L_x = 500$ km, $W = 40$ km, $A = 1.25 \times 10^{-25}$ $\mathrm{Pa}^{-3}\mathrm{s}^{-1}$, and accumulation rate $a = 0.3$ ma^{-1}. Density of ice and seawater were, $\rho = 917$ kg m^{-3} and $\rho = 1028$ kg m^{-3}, respectively. The bed profile was

$$R(x,y) = -\frac{\rho}{\rho_w} 1000 \text{ m} - 0.3(L_x - x). \tag{28}$$

Notice that the bottom slope (0.3) is greater than those in the Buttressing experiments detailed above, and also that there is no continental shelf break. The Dupont and Alley model also differed in that they used a linear basal friction parameterization, so we did the same by setting $m = 1$ in (10). The initial profile was of the form (26), with $x_g = 380$ km.

[86] Figure 12 shows the results of our simulation. After about 1000 years the model converged to a steady state, shown in Figures 12a (profile) and 12a (top-down view). The length of the shelf is about 12 km, which is roughly like the configurations found in the Dupont and Alley. (The fact that agreement is not better is not serious; we did not seek to reproduce their results, but rather explore a sector of parameter space different than that examined in our Buttressing experiments above to investigate stabilization through buttressing.) Figure 12c simply shows evolution of *VAF* to demonstrate that a steady state was reached.

[87] Note that the lateral corners of the ice shelf have become grounded, affecting the thickness at those corners. We believe these features are robust; the no-slip sidewalls imply that mass will build up more at the sides of the shelf front than at the center, and the shelf is already very thick compared to the ocean depth as seen from Figure 12a. The fact that the shelf front is partially grounded does not affect the boundary condition there, because the correction (7) to (6) accounts for this.

[88] Note also that the patches of grounded ice at the corners of the shelf have the effect of introducing additional frictional stress, as well as decreasing the lateral shelf area available for buttressing. However, taking into account the small areas of the patches and the relatively weak frictional properties of the bed, we estimate these quantities to be much smaller than the total buttressing force exerted by the shelf [*Dupont*, 2004], and so we do not believe that they play a dynamic role.

5.3. Ice Rise

[89] All the experiments discussed so far involve bedrock profiles that are homogeneous in y, but our methods allow for inhomogeneities in the transverse direction and multiple grounding line topologies. We investigate the effect of a localized area of grounding on the dynamics of a marine ice sheet. Such ice rises are thought to play a dynamic role in marine ice sheets along with sidewall buttressing [*Thomas*, 1979].

[90] In this experiment we force the ice shelf to become grounded at a point by introducing a localized seamount on a foredeepened bed such that the peak of the seamount is below sea level. The domain is 1500 km long as before with width $W = 550$ km. The bed is given by $R(x, y) = R_0(x, y) + R_{mount}(x, y)$, where $R_0(x, y)$ is given by (28) with slope 0.5×10^{-3}. R_{mount} is nonzero only in the subdomain 1.2×10^6 m

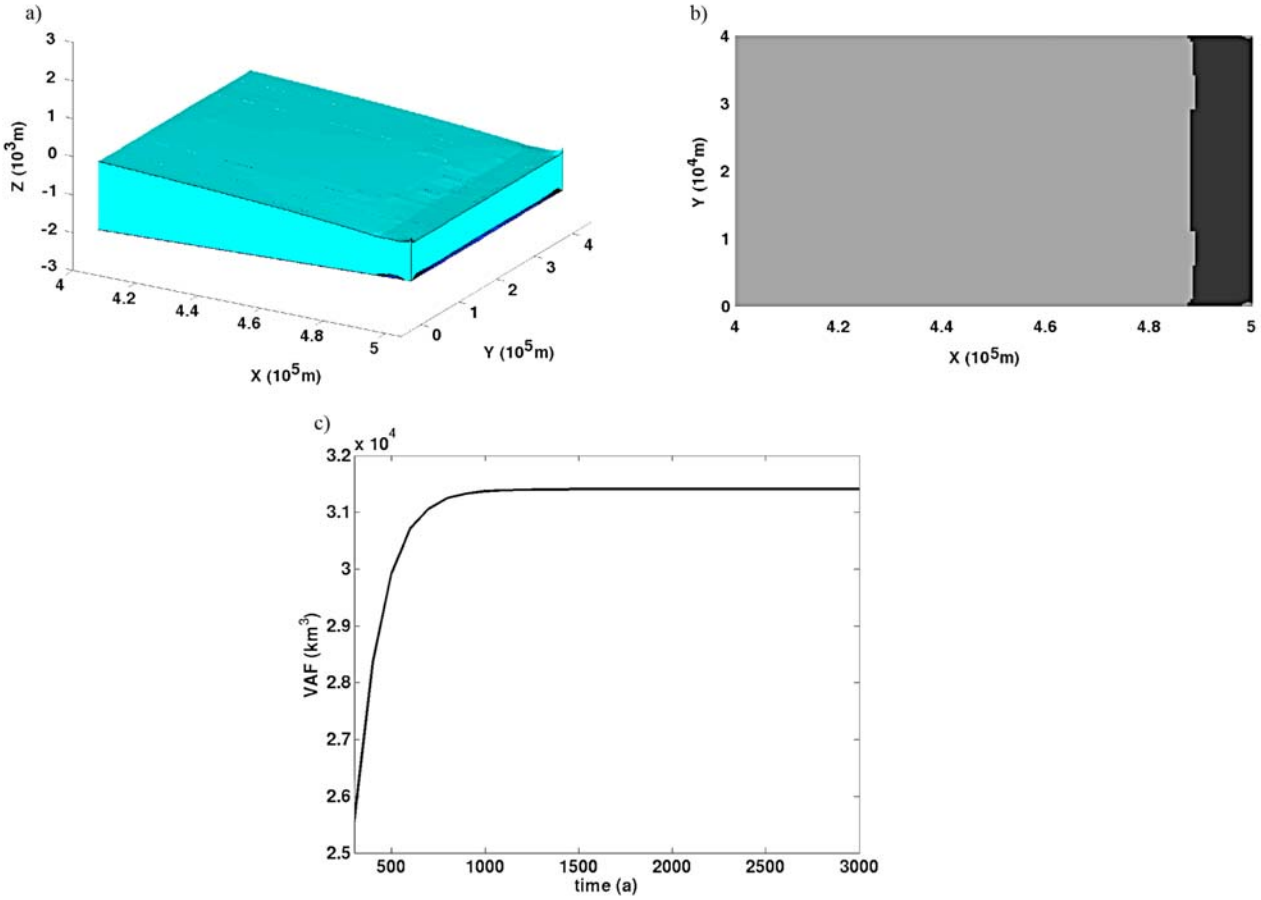

Figure 12. Ice rise experiment. (a) Profile of marine ice sheet once it has reached steady state. Note that the entire sheet is not displayed, only the portion up to 100 km inland from the shelf front, which represents the domain considered by *Dupont and Alley* [2005]. (b) Top-down view of Figure 12a. Light grey indicates grounded ice, and floating regions are dark. (c) Evolution of *VAF* over time, indicating steady state.

$\leq x \leq 1.4 \times 10^6$ m, $W/2 - 10^5$ m $\leq y \leq W/2 + 10^5$ m, and has the form

$$R_{mount}(x,y) = h_{mount}\cos\left(\frac{\pi}{10^5\text{m}}\left(x - 1.3 \times 10^6\text{m}\right)\right) \cdot \cos\left(\frac{\pi}{10^5\text{m}}(y - W/2)\right). \quad (29)$$

This amounts to a tensor-defined cosine hill 200 km wide, centered 200 km from the ice shelf front. h_{mount}, the height of the seamount, is 490 m, chosen so that it just touches the base of the shelf in the initial condition, defined by (26) with x_g = 1000 km. Glen's Law constant, basal friction coefficient, and accumulation are $1.5 \times 10^{-25}\text{Pa}^{-3}\text{s}^{-1}$, 7.6×10^6 Pa $(\text{m}^{-1}\text{s})^{1/3}$, and 0.3 ma^{-1}, respectively. From Figure 11 we see that with an initial condition as in the previous conditions, such a sheet will collapse in about 3 ka with a *y*-homogeneous bed. Figure 13a shows a profile of the sheet. Half of the sheet is cut away so the seamount can be seen. We found that, rather than collapse, the sheet advanced until the grounding line was past the seamount, although this process was very slow, much slower than collapse in an equivalent ice rise–free simulation.

[91] Figure 13b is a map of the domain showing the grounded portion of the domain (light grey) after 1 ka. Figure 13c shows *x* velocity at the same time and illustrates the dynamic effect of the rise. The shelf directly upstream of the rise appears shielded from the calving front and velocity is lower there than to either side. Ultimately the region between the seamount and the "main" grounding line (the one that intersects the sides in Figure 13b) became grounded and the 2 branches of the grounding line coalesce. Figure 13d shows the grounded domain after 15 ka, just after this has happened.

[92] Eventually, the grounding line moves all the way to shelf front and the sheet is completely grounded, similar to unstable advance over a foredeepened bed. It is curious that adding the seamount has the same long-term effect as halving the domain width, that is, to turn unstable retreat into slow but unstable advance. This suggests that such bed topography effectively decreases shelf width, with the rise acting as a rigid sidewall to each half width and increasing the level of buttressing. Figure 13c supports this idea, as the

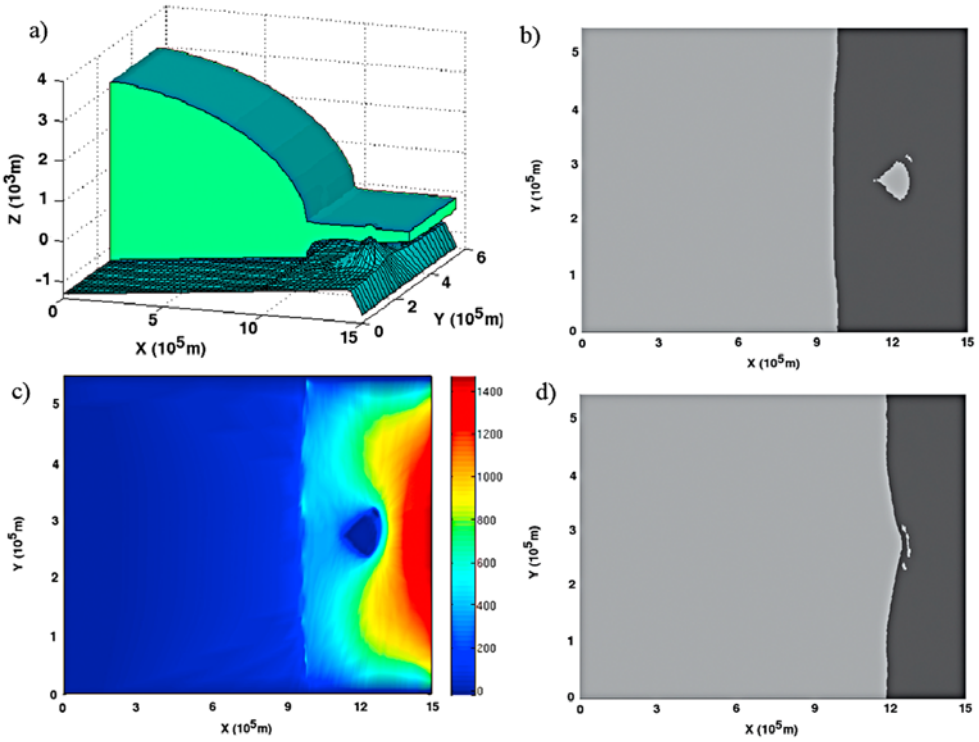

Figure 13. Ice rise experiment. (a) Marine ice sheet with partly grounded shelf (ice rise). The sheet is cut away to reveal the seamount. (b) Domain after 1 ka. Light grey indicates grounded ice, and floating regions are dark. (c) The x-velocity (ma^{-1}) at 1 ka. (d) Domain after 15 ka. The two grounded areas have merged.

velocity field on either side of the rise is similar to that in a shelf without an ice rise.

6. Discussion of 2-D Results

6.1. Performance of Mesh Adaption

[93] Our experiments allowed us to observe the effectiveness of each of our mesh adaption schemes over a wide range of parameters. This was important because the moving mesh scheme was initially developed to handle the stress regime transition across the grounding line in a 1-D flow line model, and the adaptive refinement scheme was also developed in anticipation of localized stress gradients. There is no doubt that in most cases some level of refinement is needed near the grounding line to resolve stresses accurately, but our results lead us to make a distinction between calculating grounding line flux, which arises from a balance of forces, and grounding line movement, which is kinematic: the floatation condition, from the point of view of the shelfy stream equations, does not depend on rheology or internal stresses. Both issues contribute to difficulties with Eulerian grounding line representation, while only the former affects ALE models, which do not generalize easily to two dimensions.

[94] We have shown that grounding line interpolation similar to *Pattyn et al.* [2006], while not resolving additional physics, allows the grounding line to move more freely and to better represent what we believe to be the true solution. When there are sharp thickness gradients at the grounding line, as occurs when there is low to moderate buttressing, our moving mesh is effective at facilitating grounding line movement, as it can provide very high resolution at the grounding line ensured by including distance from the grounding line or height above flotation in the monitor function. Our adaptive refinement model, on the other hand, did not perform as well as the moving mesh model in the downsloping bed experiments. This may be due to insufficient resolution for grounding line movement: the scheme uses a constraint on the total number of cells, and high resolution elsewhere, such as the shelf margin near calving front, leaves fewer cells available for the transition zone. This was not an issue in the 1-D adaptive refinement simulations, as there was no shelf margin demanding high resolution at the expense of the grounding line region.

[95] On the other hand, there is mesh distortion in the moving mesh scheme, which can degrade the numerical solution. In Figures 7b and 7d some distortion can be seen where the grounding line intersects the sidewalls. With buttressing playing a small role inaccuracies in this region are probably not detrimental to the overall solution, but for very narrow domains we found that the mesh becomes very badly distorted across the entire transverse width of the domain. This may be because lateral shearing is poorly resolved, which could result in spurious thickness evolution and degrade the numerical solution even further due to the dependence of the mesh-moving scheme on the thickness field. By contrast, in narrow domains the adaptive refinement scheme focused resolution along the margins of the sheet and the shelf and at the calving front, not at the grounding line. For these domains, the adaptive refinement

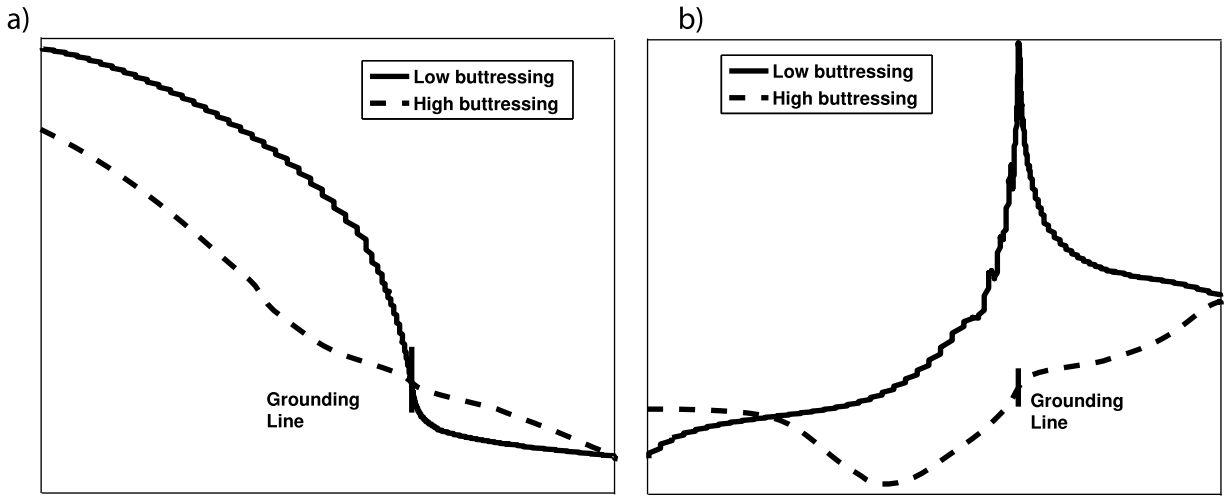

Figure 14. Regime comparison of high and low buttressing. Low buttressing (marine ice sheet in a wide channel) is characterized by high gradients in thickness and longitudinal stress at the grounding line and high buttressing (narrow channel) by a smaller grounding line thickness gradient, thicker ice shelf, and less localized longitudinal stress profile. (a) Thickness along the center-line. (b) Longitudinal stress along the center-line.

results were used for the data in Figure 11. (For a specific set of parameter values for which this was done, agreement of the solution with a very high-resolution uniform mesh simulation was found to be satisfactory.)

[96] Figure 14 illustrates the difference between the low-buttressing (wide domain) and high-buttressing (narrow domain) case with respect to thickness profile and longitudinal stress. Figure 14a compares the center line thicknesses from two representative simulations. In the low-buttressed profile there is a sharp thickness gradient at the grounding line. Figure 14b shows center line longitudinal stress. The key point of the stress profiles is that in the low-buttressed case, the only part of the domain that contains high stress gradients is near the grounding line, and so a mesh adaption scheme which seeks to capture steep stress gradients can do so by adding resolution near the grounding line. While shear stress is not shown, its presence in the high-buttressing case can be inferred from the drop in longitudinal stress upstream of the grounding line. Clearly a mesh adaption scheme which only resolves highly around the grounding line will miss some of the features in the stress field.

[97] This highlights the main difference between the moving mesh scheme and the adaptive refinement scheme: in the former we tell the model where we think resolution is needed, albeit in an indirect way, while in the latter the model decides where to resolve based on the solution itself, allowing for more flexibility. This flexibility makes adaptive refinement a more potentially attractive form of mesh adaption, since there may be features aside from the grounding line that require higher resolution than the majority of the domain. Also, adaptive refinement, with its regularly shaped cells, would probably be more amenable to interpolation of data to and from the grid, for the purposes of forcing and maybe coupling with other models. Still, our adaptive refinement model did not perform as well as our moving mesh model in terms of grounding line movement because of the sharp change in thickness near the grounding line, which leads to difficulties in making the grounding line move, especially if it is restricted numerically to lie along cell boundaries. However, it may be possible to solve this issue by augmenting the error estimator (23) with a cost function based on thickness gradient. Further development of the adaptive refinement scheme is planned.

6.2. Marine Ice Sheet Stability

[98] Buttressing is the effect of tangential stress on the sidewalls. In the context of our nondimensionalized system (12), and ignoring along-flow gradients in transverse velocities, this tangential stress at a point on the sidewalls will be approximately [*Dupont and Alley*, 2005]

$$\tau_{tangent} \equiv \varepsilon \int_{x_g}^{x_c} \frac{\hat{h}\hat{u}^{\frac{1}{n}}}{\left(\frac{\hat{W}}{2}\right)^{1+\frac{1}{n}}} \mathrm{d}\hat{x}, \tag{30}$$

where $\hat{W}$ is the width of the channel divided by the length scale, and the integral is from the grounding line to the calving front. The integrand is actually very similar to the basal stress term $\hat{u}^m$ when $m = \frac{1}{3}$, although the coefficient of $\hat{u}^{\frac{1}{n}}$ is usually smaller than 1. In general $\tau_{tangent}$ increases with grounding line retreat, although the specifics depend on shelf geometry. $\tau_{tangent}$, along with longitudinal stress

$$\tau_{long} \equiv \hat{\nu}\hat{h}\left(4\hat{u}_{\hat{x}} + 2\hat{u}_{\hat{y}}\right), \tag{31}$$

balances the integrated driving force of the shelf,

$$\tau_{driving} \equiv \frac{1}{2}\left(1 - \frac{\rho}{\rho_w}\right)\hat{h}_g^2, \tag{32}$$

where $\hat{h}_g$ is thickness at the grounding line. (Note $\tau_{tangent}$ has been divided by $\hat{W}$ to compare with $\tau_{driving}$ and τ_{long}.)

[99] In the case of an unbuttressed marine ice sheet on a foredeepened bed, instability arises because grounding line flux increases with depth. According to the analysis of *Schoof* [2007a], the strong dependence of flux on grounding line depth is actually related to a strong dependence of flux on longitudinal stress (τ_{long}). Therefore it might be possible in some cases that in a buttressed shelf, $\tau_{tangent}$ balances $\tau_{driving}$ enough to lessen τ_{long}, and perhaps for τ_{long} to decrease as the grounding line retreats, at least locally. Were this to happen it would be when $\hat{W}$ is very small and ε is relatively large (for instance, in the case of a weak bed).

[100] This stability reversal did not seem to occur for most of our experiments over a foredeepened bed, although it was observed in one experiment, in which model parameters were very different from the rest of the experiments and similar to those used by *Dupont and Alley* [2005]. The main parameter differences were a narrower channel and a basal friction coefficient that yielded much lower basal stress, as well as a much steeper bed. This behavioral difference may be indicative of a regime change between control by longitudinal stresses and control by tangential stresses. It can be shown [*Schoof*, 2007a] that the factor $\varepsilon/\left(\frac{\hat{W}}{2}\right)^{1+\frac{1}{n}}$ in (30) is at least an order of magnitude larger in the experiments using parameters from Dupont and Alley than in the other experiments. With $\tau_{tangent}$ playing a larger role in the force balance and increasing with the length of the ice shelf, this could explain the stability found in the former. Certainly further investigation is warranted.

[101] If we consider the implications of our simulations on a foredeepened bed for real Antarctic stream shelf systems, we may draw the conclusion that sheets in narrow embayments with relatively weak beds, such as Pine Island or Thwaites glaciers, are stabilized by buttressing. Meanwhile larger embayments with higher basal friction coefficients, such as the Filchner-Ronne embayment [*Frolich et al.*, 1987; *Frolich and Doake*, 1988], are controlled by longitudinal stresses in the transition zone. These shelf stream systems, therefore, are either unstable (or metastable) on time scales much longer than our current observations have been able to detect, or are stabilized by means not considered in this study. Regardless of stability, though, both types of stream shelf systems would be subject to relatively rapid change were their shelves to disintegrate or thin dramatically.

7. Conclusions

[102] In numerical solutions of marine ice sheet dynamics, insufficient resolution near the grounding line frequently gives rise to numerical artifacts and may give results that are not only quantitatively incorrect, but also qualitatively misleading [e.g., *Vieli and Payne*, 2005].

[103] Using a flow line model that solves the shelfy stream equations for a marine ice sheet with a moving grounding line, we have shown that two different mesh adaption techniques, moving mesh (r refinement) and adaptive refinement (h refinement), provide an accurate solution while using far less computational resources than would be required using a uniformly spaced grid. Both mesh adaption schemes evolve the grid in time; the moving mesh according to grounding line position and adaptive refinement according to gradients in the strain rate field. Both extend to two horizontal dimensions and allow for grounding lines of changing topology, such as formation and elimination of ice rises.

[104] These advances in model numerics have allowed us to investigate the effect of ice shelf buttressing on marine ice sheet dynamics in detail. For downsloping beds, our model generates equilibrium profiles that are unique for a given set of model parameters (including geometrical parameters controlling buttressing, such as ice shelf width), and the model also shows that these equilibrium shapes are reached eventually regardless of initial conditions. This is essentially an extension of the corresponding result for unbuttressed one-dimensional sheet shelf systems [e.g., *Weertman*, 1974; *Schoof*, 2007a].

[105] In experiments with a 2-D marine ice sheet in a channel over a foredeepened (upward-sloping) bed, we generally found that the sheet was unstable and that its behavior was dependent on the initial condition, which is again qualitatively like the unbuttressed case. This instability was seen even when the channel width was small (about 10% of its length) and buttressing was high. However, the eventual collapse of the sheet was greatly delayed. Still, we were also able to find a parameter regime in which the shelf was able to stabilize the marine ice sheet with its grounding line on a foredeepened bed; in line with previous results from a simpler model in which the lateral direction was parameterized [*Dupont and Alley*, 2005], this occurred in a narrow channel with a steep bottom slope and a relatively weak bed. From our experiments we draw the conclusions that narrower, lower-traction marine streams like Pine Island Glacier are likely stabilized by ice shelves, but streams in larger embayments, like those feeding the Filchner-Ronne shelf, are possibly unstable, albeit on very long time scales.

[106] Finally, we ran a simulation with a generally foredeepened bed profile that also contained a seamount transverse to the flow. It was seen that contact of the shelf with the seamount was enough to prevent collapse of the sheet, and to switch its behavior to grounding line advance instead, underlining the potentially significant role of ice rises (such as Berkner Island in the Filchner-Ronne ice shelf) in marine ice sheet dynamics. The response was in fact similar to that of a much narrower sheet, suggesting that ice rises effectively narrow the flow channel. However, further work is needed to investigate the effects of irregular bed topographies.

[107] Our model runs have also allowed us to assess the performance of our mesh refinement methods in more detail, which provides some insight into possible avenues for future improvement. In our 2-D simulations of a marine ice sheet (i.e., with two horizontal dimensions) in a channel with rigid walls, our moving mesh scheme worked well when the width of the channel was larger than roughly 30% of its length. On a downsloping bed, a unique, stable steady state was exhibited, in qualitative agreement with the dynamics of an unbuttressed sheet. It was shown that this steady state was robust under a uniform increase in grid resolution. However, for narrow channel widths the moving mesh scheme tended to distort the mesh, and this affected the simulation. Conversely, the adaptive refinement scheme did not perform as well as the moving mesh for wide-

channel simulations, but its performance improved when the channel was narrowed, and buttressing reduced longitudinal stresses at the grounding line.

[108] The differences in performance can be attributed to differences in stress regimes. In the case of moderate channel width, there is low buttressing and the stress profile is similar to that of the unbuttressed case, with a high longitudinal stress gradient at the grounding line along with a large thickness gradient. In this regime the shear margins are probably not that important to resolve and a scheme that puts the highest resolution at the grounding line, such as the moving mesh, performs well. However, in a narrow channel the shear margins are important, and a reduction of longitudinal stress at the grounding line is accompanied by a reduced thickness gradient. In this case an adaption scheme based on strain rate gradients is more effective.

[109] We would like an adaption scheme that handles both regimes. Adaptive refinement is the better candidate for improvement because it does not make a priori assumptions about where resolution is needed, and because it would be more amenable to interpolation in a coupling or forcing scheme. As a possible way ahead, we propose that the adaptive refinement scheme be augmented with a cost associated with either thickness gradients or grounding line proximity.

[110] We point out that, in addition to the aforementioned advantages, adaptive refinement is potentially very beneficial to the modeling of ice streams (and ice sheets as well). Transient features requiring resolution than cannot be allowed for globally must be accounted for by glaciological models, and are not limited to grounding line transition zones. Ice stream shear margins can migrate and basal conditions can change, possibly requiring changes in horizontal resolution (and, in higher-order models, changes in vertical resolution accompanying the transition between from sheet to stream flow).

[111] **Acknowledgments.** We acknowledge the efforts of our Editor and three reviewers in improving the clarity of the final manuscript. This work was made possible by the NASA Earth Science Fellowship, the NYU Dean's Dissertation Fellowship, the Canada Research Chair at the University of British Columbia, NASA grants NNX08AN52G and NNX07AU53G, DOE grant DE-FG02-08ER64587, NSF grants ANT-0732869 and ARC-0806393, and NSERC Discovery grant 357193-08.

References

Beckett, G., J. A. Mackenzie, and M. L. Robertson (2001), A moving mesh finite element method for the solution of two-dimensional Stefan problems, *J. Comput. Phys.*, *168*, 500–518.

Blatter, H. (1995), Velocity and stress fields in grounded glaciers: A simple algorithm for including deviatoric stress gradients, *J. Glaciol.*, *41*, 333–344.

Chugunov, V. A., and A. V. Wilchinsky (1996), Modelling of a marine glacier and ice-sheet-ice-shelf transition zone based on asymptotic analysis, *Ann. Glaciol.*, *23*, 59–67.

Dupont, T. K. (2004), Abrupt changes in ice shelves and ice streams: Model studies, Ph.D. thesis, Penn. State Univ., State College.

Dupont, T. K., and R. Alley (2005), Assessment of the importance of ice-shelf buttressing to ice-sheet flow, *Geophys. Res. Lett.*, *32*, L04503, doi:10.1029/2004GL022024.

Evans, L. C. (1991), *Partial Differential Equations*, Am. Math. Soc., Providence, R. I.

Fowler, A. C. (1981), A theoretical treatment of the sliding of glaciers in the absence of cavitation, *Philos. Trans. R. Soc. London, Ser. A*, *298*, 637–681.

Frolich, R. M., and C. S. M. Doake (1988), Relative importance of lateral and vertical shear on Rutford Ice Stream, Antarctica, *Ann. Glaciol.*, *11*, 19–22.

Frolich, R. M., D. R. Mantripp, D. G. Vaughan, and C. S. M. Doake (1987), Force balance of Rutford Ice Stream, Antarctica, *IAHS Publ, 170*, 323–331.

Hindmarsh, R. (1996), Stability of ice-rises and uncoupled marine ice-sheets, *Ann. Glaciol.*, *23*, 105–115.

Holland, D. M., R. H. Thomas, B. de Young, M. Ribergaard, and B. Lyberth (2008), Acceleration of Jakobshavn Isbrae triggered by warm subsurface ocean waters, *Nat. Geosci.*, *1*, 659–664.

Hulbe, C. (1998), Heat balance of West Antarctic ice streams, investigated with a numerical model of coupled ice sheet, ice stream, and ice shelf flow, Ph.D. thesis, Univ. of Chicago, Chicago, Ill.

Huybrechts, P. (1990), A 3-D model for the Antarctic ice sheet: A sensitivity study on the glacial-interglacial contrast, *Clim. Dyn.*, *5*, 79–92.

Jenkins, A., and D. M. Holland (2007), Melting of floating ice and sea level rise, *Geophys. Res. Lett.*, *34*, L16609, doi:10.1029/2007GL030784.

Joughin, I., W. Abdalati, and M. Fahnestock (2004), Large fluctuations in speed on Greenland's Jakobshavn Isbrae glacier, *Nature*, *432*, 608–610.

Kelly, D. W., J. R. Gago, O. C. Zienkiewicz, and I. Babuska (1983), A posteriori error analysis and adaptive processes in the finite element method. Part I. Error analysis, *Int. J. Numer. Methods Eng.*, *19*, 1593–1619.

Krabill, W., et al. (2000), Greenland ice sheet: High-elevation balance and peripheral thinning, *Science*, *289*, 428–430.

Lax, P. D., and R. D. Richtmeyer (1956), Survey of the stability of linear finite difference equations, *Commun. Pure Appl. Math.*, *9*, 267–293.

MacAyeal, D. R. (1989), Large-scale ice flow over a viscous basal sediment: Theory and application to Ice Stream B, Antarctica, *J. Geophys. Res.*, *94*, 4071–4087.

MacAyeal, D. R., and V. Barcilon (1988), Ice-shelf response to ice-stream discharge fluctuations: I. Unconfined ice tongues, *J. Glaciol.*, *34*, 121–127.

MacAyeal, D. R., and R. H. Thomas (1986), The effects of basal melting on the present flow of the Ross Ice Shelf, Antarctica, *J. Glaciol.*, *32*, 72–86.

Mayer, C., and P. Huybrechts (1999), Ice-dynamic conditions across the grounding zone, Ekstromisen, East Antarctica, *J. Glaciol.*, *45*, 384–393.

Mercer, J. (1978), West Antarctic Ice Sheet and CO2 greenhouse effect: A threat of disaster, *Nature*, *271*, 321–325.

Nowicki, S. M. J., and D. J. Wingham (2007), Conditions for a steady ice sheet-ice shelf junction, *Earth Planet. Sci. Lett.*, *265*, 246–255.

Paterson, W. S. B. (2001), *The Physics of Glaciers*, 3rd ed., Butterworth-Heinemann, Oxford, U. K.

Pattyn, F. (2002), Transient glacier response with a higher-order numerical ice-flow model, *J. Glaciol.*, *48*, 467–477.

Pattyn, F., A. Huyghe, S. D. Brabander, and B. D. Smedt (2006), The role of transition zones in marine ice sheet dynamics, *J. Geophys. Res.*, *111*, F02004, doi:10.1029/2005JF000394.

Payne, A. J., A. Veili, A. Shepherd, D. J. Wingham, and E. Rignot (2004), Recent dramatic thinning of largest West Antarctic ice stream triggered by oceans, *Geophys. Res. Lett.*, *31*, L23401, doi:10.1029/2004GL021284.

Reist, A. (2005), Mathematical analysis and numerical simulation of the motion of a glacier, Ph.D. thesis, Ecole Polytech. Fed. de Lausanne, Lausanne, Switzerland.

Rignot, E., D. G. Vaughan, M. Schmeltz, T. K. Dupont, and D. R. MacAyeal (2002), Acceleration of Pine Island and Thwaites glaciers, West Antarctica, *Ann. Glaciol.*, *34*, 189–194.

Schmeltz, M., E. Rignot, T. K. Dupont, and D. R. Macayeal (2002), Sensitivity of Pine Island Glacier, West Antarctica, to changes in ice-shelf and basal conditions: A model study, *J. Glaciol.*, *48*, 552–558.

Schoof, C. (2006), A variational approach to ice stream flow, *J. Fluid Mech.*, *556*, 227–251.

Schoof, C. (2007a), Marine ice sheet dynamics. Part I. The case of rapid sliding, *J. Fluid Mech.*, *573*, 27–55.

Schoof, C. (2007b), Ice sheet grounding line dynamics: Steady states, stability, and hysteresis, *J. Geophys. Res.*, *112*, F03238, doi:10.1029/2006JF000664.

Schoof, C. (2009), Coulomb friction and other sliding laws in a higher-order glacier flow model, *Math. Models Methods Appl. Sci.*, in press.

Shepherd, A., and D. J. Wingham (2007), Recent sea-level contributions of the Antarctic and Greenland ice sheets, *Science*, *315*, 1529–1532.

Shepherd, A., D. J. Wingham, and J. Mansley (2002), Inland thinning of the Amundsen Sea sector, West Antarctica, *Geophys. Res. Lett.*, *29*(10), 1364, doi:10.1029/2001GL014183.

Shepherd, A., D. J. Wingham, and E. Rignot (2004), Warm ocean is eroding West Antarctic Ice Sheet, *Geophys. Res. Lett.*, *31*, L23402, doi:10.1029/2004GL021106.

Tan, Z. (2007), Adaptive moving mesh methods for two-dimensional resistive magneto-hydrodynamic PDE models, *Comput. Fluids*, *36*, 758–771.

Thomas, R. H. (1977), Calving bay dynamics and ice-sheet retreat up the St. Lawrence Valley System, *Geogr. Phys. Quat.*, *31*, 347–356.
Thomas, R. H. (1979), The dynamics of marine ice sheets, *J. Glaciol.*, *31*, 347–356.
Thomas, R. H. (1985), Responses of the polar ice sheets to climatic warming, in Glaciers, ice sheets and sea level: Effects of a CO2-induced climatic change, *Rep. DOE/ER/60235-1*, pp. 301–316, Dep. of Energy, Washington, D. C.
Thomas, R. H., and C. R. Bentley (1978), A model for the Holocene retreat of the West Antarctic Ice Sheet, *Quat. Res.*, *10*, 150–170.
Van der Veen, C. J. (1985), Response of a marine ice sheet to changes at the grounding line, *Quat. Res.*, *24*, 257–267.
Van der Veen, C. J. (1999), *Fundamentals of Glacier Dynamics*, A. A. Balkema, Netherlands.
Vieli, A., and A. J. Payne (2005), Assessing the ability of numerical ice sheet models to simulate grounding line migration, *J. Geophys. Res.*, *110*, F01003, doi:10.1029/2004JF000202.
Weertman, J. (1974), Stability of the junction of an ice sheet and an ice shelf, *J. Glaciol.*, *13*, 3–11.
Wilchinsky, A. V., and V. A. Chugunov (2000), Ice-stream-ice-shelf transition: Theoretical analysis of two-dimensional flow, *Ann. Glaciol.*, *30*, 153–162.

D. Goldberg and D. M. Holland, Courant Institute of Mathematical Sciences, New York University, 251 Mercer Street, New York, NY 10012, USA. (dgoldberg@cims.nyu.edu)
C. Schoof, Department of Earth and Ocean Sciences, University of British Columbia, Vancouver, BC V6T 1Z4, Canada.